annalen der physik
www.ann-phys.org

Modeling Communicable Diseases, Human Mobility, and Epidemics: A Review

David Soriano-Paños, Wesley Cota, Silvio C. Ferreira, Gourab Ghoshal, Alex Arenas,* and Jesús Gómez-Gardeñes**

The spatiotemporal propagation patterns of recent infectious diseases, originated as localized epidemic outbreaks and eventually becoming global pandemics, are highly influenced by human mobility. Case exportation from endemic areas to the rest of the countries has become unavoidable because of the striking growth of the global mobility network, helping to overcome the physical distance existing between faraway regions. In this context, understanding the features driving contagions upon the arrival of an index case in local environments constitutes an essential task to devise policies aimed at avoiding the community transmission of these diseases and the subsequent case exportation to other unaffected areas. In this review, an overview of the different models addressing this topic is given, focusing on the movement–interaction–return model and different subsequent frameworks introduced to explain the complex interplay between the recurrent movements and contagion dynamics.

1. Introduction

The global spread of communicable diseases can be conceived as a reaction-diffusion process where the reaction stage corresponds to the contagions between infectious hosts and susceptible individuals and the diffusion stage is associated with the movements of the hosts, fostering the spatial dissemination of pathogens. A comparison of the evolution of modern epidemics and those that occurred before the 20th century reveals a very significant difference: there has been an inversion of the time scales associated with the processes governing the spread of diseases. In terms of reaction–diffusion processes, pandemics occurring before the 20th century, like the Black Death,[1] were characterized by diffusion times much slower than the reaction time scales, which gave rise to well-defined subsequent epidemic outbreaks, happening one after another, being propagated typically to geographically neighboring areas or as dictated by the most usual trading routes. In contrast, recent major epidemics, such as Influenza A in 2009 or much more recently the COVID-19 pandemic, have been characterized by major outbreaks occurring simultaneously in distant regions as a consequence of the shortening of the time scale associated with diffusion processes. In particular, the progressive shortening of the time scales governing human mobility has made it possible for a person to visit different regions during her infectious period, resulting in the aforementioned temporal inversion between the time scales corresponding to the reaction and diffusion.

One of the major drivers behind the acceleration of the spatial dissemination of recent epidemic outbreaks is the striking growth experienced by the airport mobility network.[2] In this sense, different studies have proven that international

D. Soriano-Paños
Instituto Gulbenkian de Ciência
Oeiras 2780-156, Portugal
E-mail: sorianopanos@gmail.com

J. Gómez-Gardeñes
Department of Condensed Matter Physics
University of Zaragoza
Zaragoza 50009, Spain
E-mail: gardenes@unizar.es

The ORCID identification number(s) for the author(s) of this article can be found under https://doi.org/10.1002/andp.202100482

DOI: 10.1002/andp.202100482

D. Soriano-Paños, J. Gómez-Gardeñes
GOTHAM Lab-Institute for Biocomputation and Physics of Complex Systems (BIFI)
University of Zaragoza
Zaragoza 50018, Spain

W. Cota, S. C. Ferreira
Departamento de Fisica
Universidade Federal de Viçosa
Viçosa, Minas Gerais 36570-900, Brazil

S. C. Ferreira
National Institute of Science and Technology for Complex Systems
Rio de Janeiro 22290-180, Brazil

G. Ghoshal
Department of Physics & Astronomy
University of Rochester
Rochester 14607, United States

A. Arenas
Departament d'Enginyeria Informàtica i Matemàtiques
Universität Rovira i Virgili
Tarragona 43007, Spain
E-mail: alexandre.arenas@urv.cat

connections provide key information to predict the global expansion of epidemic outbreaks initially localized in small geographical areas. For instance, the airport connectivity has proved to be a very reliable proxy to estimate the arrival times of SARS epidemic to different countries in 2003,[3,4] the most likely infectious routes followed by influenza virus H1N1 in 2009,[5] or, more recently, the risk of importing COVID-19 cases.[6,7]

Unlike the well-defined role of the airport mobility network for the importation and exportation of cases, solving the complex relationship existing between the distribution of the population across a city, their recurrent commuting patterns and the evolution of local outbreaks remains an open challenge. In this sense, several examples addressing the impact of daily recurrent mobility on the spread of contagious diseases can be found in the literature.[8–13] Despite the theoretical flavor of most of these works, the recent advances in data gathering techniques[14–16] has enabled to capture realistically the daily urban rhythms of the population and to evaluate to what extent they provide useful information to characterize local outbreaks. Indeed, local mobility patterns have been already useful for identifying the most exposed areas in some epidemic scenarios[17] as well as reproducing the infection routes of H1N1 influenza,[5] Malaria,[18] and SARS-CoV-2.[19–22] All these theoretical and applied works rely on metapopulation architectures to simultaneously capture the population movements and those microscopic processes driving the spread of diseases.

In this review, we provide a broad overview of the different theoretical models tackling the interplay between recurrent mobility and epidemic spreading on metapopulations. Some basic notions about metapopulations and how to construct them synthetically are explained in Section 2, while in Section 3 we summarize the integration of epidemic spread in metapopulation dynamics relying on heterogeneous mean-field approaches. In Section 4, we present the theoretical core of this review, the movement–interaction–return (MIR) model. The application of the MIR model in real metapopulations reveals that the impact of human movements is not universal and leads to the so-called epidemic detriment, for which restricting mobility may not be beneficial to contain an ongoing outbreak. Section 5 is fully-devoted to the characterization and understanding of this phenomenon, concluding with some examples on simple networked systems. Finally, in Section 6, we show how the equations of the MIR model and the theoretical knowledge on the origin of the epidemic detriment on synthetic networks have been leveraged to design surgical interventions reducing cities' vulnerability to epidemic outbreaks.

Finally, along the review we will focus on the paradigmatic susceptible-infected-susceptible (SIS) and susceptible-infected-recovered (SIR) models, as they are the simplest frameworks capturing the transition between the disease-free and the epidemic states. The SIS and SIR models are characterized by just two parameters, λ and μ, which accounts for the contagion probability when a susceptible agent meets an infected one and the recovery probability of infecteds respectively. The difference between SIS and SIR models resides in the evolution of those infected agents that recover, becoming again susceptible in the SIS case while passing to a recovered state that cannot contract/transmit the disease in the SIR one. The dynamical simplicity of these frameworks allows us to put the emphasis on the incorporation of human recurrent mobility patterns into the complete formalism, although the phenomenology here described can be generally extended to more refined and realistic epidemic models.

2. Metapopulations

Metapopulations were initially introduced in the field of ecology to study the viability of the coexistence of different species in spatially distributed ecosystems.[23–26] On general grounds, a metapopulation is defined as a set of spatially separated subpopulations which interact among each other because of the mobility of their constituents. In the language used in network science, the usual representation of a metapopulation is a complex network where each node, usually referred to as patch, corresponds to the geographical area populated by each subpopulation. In its turn, the links connecting the different subpopulations now encode the mobility patterns of the population rather than their interaction patterns. Formally, a metapopulation with N_P patches and L links is defined as a tuple $\mathcal{G} = (V, N, E)$, being $V = \{v_1, \dots, v_{N_P}\}$ the set of patches in the metapopulation, $N = \{n_1, \dots, n_{N_P}\}$ the sizes of the different subpopulations and $E = \{e_1, \dots, e_L\}$ the set of edges governing the movements of the agents. For the sake of illustration, we represent a toy metapopulation with $N_P = 5$ patches in **Figure 1**.

Given their nature, metapopulations provide an useful structural backbone to incorporate reaction–diffusion processes, where reaction processes constitute the internal dynamics of each subpopulation and diffusion processes are captured by the exchange of individuals between subpopulations governed by their links. In this sense, metapopulations have allowed for studying very diverse phenomena ranging from the stability of ecosystems[27] and the dynamics determining the conservation or extinction of species[28,29] to the diffusion of tumor cells.[30] In the context of mathematical epidemiology, the use of metapopulations has constituted an important step forward in the process to turn simple epidemic models into valuable forecasting tools to anticipate the trajectory of outbreaks and devise interventions to mitigate them.[31,32] It is worth remarking that metapopulations offer a versatile framework for epidemic modeling. Depending on the patch definition, metapopulations have allowed characterizing the spread of infectious diseases across different spatial scales, ranging from a set of neighborhoods within a city to the diffusion of cases across different countries worldwide.[33–35]

2.1. Mobility Frameworks

Regardless of its spatial granularity, to run an epidemic model on top of a metapopulation, one has to choose how the mobility patterns and the diffusive behavior of the different subpopulations are introduced. In absence of data, one has also to determine how these links are synthetically constructed given the attributes of the different subpopulations exchanging individuals. Different alternatives have been proposed in the literature[36] but the most paradigmatic ones are:

- Gravity model: Inspired by the Newton's laws for body motion, the gravity model for human mobility was first introduced by George K. Zipf in 1946.[37] In this model, it is assumed that

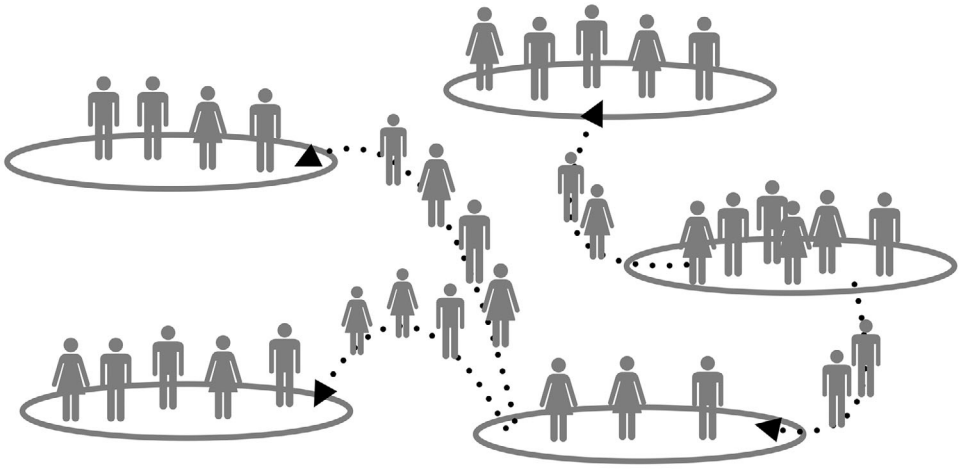

Figure 1. Schematic representation of a metapopulation with $N_P = 5$ nodes (patches) representing different geographical areas and $L = 4$ links governing the movements of the population.

the population flow between two locations is directly proportional to the product of their populations and inversely proportional to the distance among them. Mathematically, denoting the population of a node i by N_i and its distance with another node j by d_{ij}, the weighted link connecting them, T_{ij}, is estimated by

$$T_{ij} = K\frac{N_i N_j}{d_{ij}^2} \tag{1}$$

- The latter expression can be generalized by assuming an arbitrary dependence on the masses (populations) and general functions to shape the relevance of geographical distances as well. Therefore, in general, the weights are computed as

$$T_{ij} = Km_i m_j f(d_{ij}) \tag{2}$$

where m_i corresponds to the mass associated with node i and $f(d_{ij})$ is a decreasing function with the distance. The choice of $f(d_{ij})$ usually ranges from power-law to exponentially decaying functions aimed at hindering the movements between faraway regions. The typical choice for these masses are the sizes of the different subpopulations of each patch, although other variables have been also explored such as their GDP per capita.[38,39]

- Radiation model: The gravity model assumes that the flows between two locations obey only physical variables but does not account for other incentives governing people's movements.[40] To incorporate the attractiveness of each location in terms of, for instance, the number of job opportunities, the authors in ref. [41] develop the so-called radiation model. In this model, it is assumed that an individual chooses the closest location to its residence which maximizes the number of available opportunities. Assuming that the number of job positions is proportional to the population in each area, the expected value for T_{ij} reads

$$\langle T_{ij}\rangle = T_i\frac{m_i n_j}{(m_i + s_{ij})(m_i + n_j + s_{ij})} \tag{3}$$

where T_i is the total number of flows departing location i, m_i, and n_j encode the population at the origin and destination respectively and s_{ij} is the total population competing for resources inside the circle centered in i with radius d_{ij}, excluding the inhabitants of both the origin and destination. This model, unlike the gravity model, introduces a less severe penalization to long-range displacements connecting distant population centers.

Although other approaches can be also adopted, see ref. [36] for a comprehensive review on the subject, radiation and gravity models are the most used frameworks to capture the essential features of human mobility in the absence of more specific data. In any case, once computed the elements of matrix **T** as provided by these models, one obtains the complete characterization of the metapopulation in terms of V, N, and E.

Apart from the choice for the weights of the links in the metapopulation, another crucial factor is the nature of the mobility scheme considered for modeling the spread of diseases across metapopulations. For instance, Tang et al. show in ref. [42] that prioritizing the shortest paths to move across a metapopulation clearly enhances epidemic diffusion. Along this line, Gómez et al. propose an information theoretic approach[43] to reconstruct the origin–destination (OD) matrix from a set of flows observed across different locations in the metapopulation, showing that epidemic trajectories are crucially altered with respect to those obtained when including raw mobility data.

3. HMF Approaches to Epidemic Modeling in Metapopulations

The seminal model introduced in refs. [44, 45] by Colizza et al. constitutes the first theoretical framework coupling the heterogeneous structure of connections of a metapopulation and the spread of diseases. The authors take advantage of the knowledge acquired in the study of random walkers dynamics on contact networks[46] and assume that individuals move randomly across

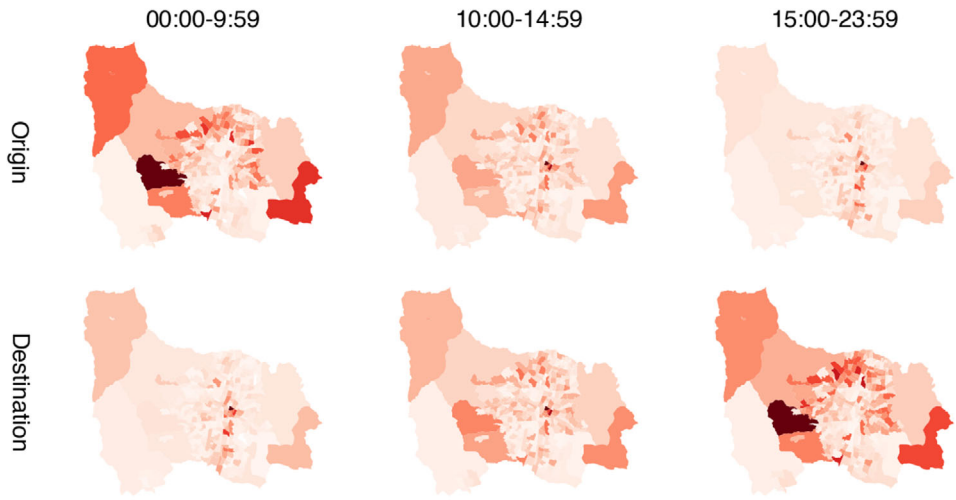

Figure 2. Origin and destination of the trips recorded in the surveys made to the population of Medellín in 2017 to characterize their mobility habits. The color of each area is proportional to the number of individuals entering (destination) or departing (origin) from it. The darker the color, the more flows are recorded for each area. The title shows the time range during which trips were aggregated. Data obtained from the authors of ref. [54].

the different patches according to the links of the metapopulation. To simplify the analysis, they also make use of a heterogeneous mean-field (HMF) approach and consider that all patches with the same number of connections are statistically equivalent. The HMF assumption in metapopulations has further implications than that included originally for contact networks,[47] for it entails that the attributes of each subpopulation, such as its size, should be linked to its connectivity in the mobility network.

Under these assumptions, and considering the SIR epidemic model, the evolution of the infected population inside patches with degree k, I_k is written as

$$\begin{aligned}\partial_t I_k = &- p_k I_k + (1-p_k)\left[-\mu I_k + \lambda \frac{I_k S_k}{N_k}\right] \\ &+ k \sum_{k'} P(k'|k) d_{k'k} \left[-\mu I_{k'} + \lambda \frac{I_{k'} S_{k'}}{N_{k'}}\right]\end{aligned} \tag{4}$$

In the latter equation, N_k represents the population inside patches with degree k, p_k the mobility rate of patches within degree class k and $d_{k'k}$ corresponds to the diffusion rate between patches with connectivities k and k'. In addition parameters λ and μ account for the contagion and recovery rates for susceptible and infectious individuals respectively.

The diffusion rate is assumed to follow the gravity model, being the masses proportional to the connectivity, so that

$$d_{k'k} \propto p_{k'} (kk')^{\theta} \tag{5}$$

Note that Equation (4) contains both reaction–diffusion processes involved in the interplay between mobility and epidemics. The evolution of the occupation of each compartment is completed with the time evolution of the spatial distribution of the population, which evolves driven by mobility as

$$\partial_t N_k(t) = -p_k N_k(t) + k \sum_{k'} P(k'|k) d_{k'k} N_{k'}(t) \tag{6}$$

Nonetheless, an usual assumption is to consider the diffusion time scales much shorter than the duration of the outbreak, so $\tau^{\text{diff}} \ll \tau^{\text{react}}$. This allows for neglecting the time evolution of the underlying populations and assume that the number of individuals inside each patch is given by the steady state of the random walker dynamics.

Apart from proposing a set of deterministic equations to track the spatio-temporal spread of diseases, the authors in ref. [45] reveal the existence of a new phase transition between the existence of localized outbreaks inside single subpopulations and the observation of widespread epidemics across the entire metapopulation. This phase transition is characterized by the so-called invasion threshold $\mathcal{R}^*$, which is computed from a branching process characterizing the evolution of the number of invaded subpopulations.

Despite the theoretical relevance or the results described above and others found in subsequent works,[5,10,31] assuming that the inhabitants of a given city behave as random walkers exploring the different neighborhoods without a fixed residence is far from reflecting the nature of our daily movements. In contrast, there is growing evidence about the prominent recurrent nature of human mobility patterns[48–51] in real datasets. As an example, we represent in **Figure 2** the results from surveys carried out in the city of Medellín in Colombia to understand the usual mobility patterns of its residents.[52,53] Specifically, we represent the volume of people arriving and departing in each specific neighborhood of the city at the beginning, middle and end of the workday. In addition to the evident distinction between residential areas and workplaces, the figure clearly suggests that urban mobility is governed by the regular trips followed by the commuters.

There are different attempts made in the literature including commuters in epidemic modeling. First works[55,56] on the topic adapt the previously explained HMF equations to include a preferential return rate τ to the associated patch of each agent, typically identified as the place where his or her residence is located. In this case, agents are not only characterized by their current location in the network but also by their associated patch,

which enlarges the set of equations needed to characterize the evolution of the population. In particular, Equation (6) turns into

$$\partial_t N_{kk}(t) = -\sigma_k N_{kk}(t) + \tau^{-1} k \sum_{k'} N_{kk'}(t) P(k'|k) \tag{7}$$

$$\partial_t N_{kk'}(t) = \sigma_{kk'} N_{kk}(t) - \tau^{-1} N_{kk'}(t) \tag{8}$$

Plugging these equations into the branching process, the authors of refs. [55, 56] derive analytically an expression that relates the invasion threshold $\mathcal{R}^*$ with the mobility rate of the population, the time scale associated with the movements and the features of the mobility network. They find that both promoting mobility and increasing the permanence times at the destinations boost epidemic spreading, for they increase the mixing between individuals from different subpopulations.

The validity of the previous findings in real metapopulations remains uncertain due to the strong theoretical assumptions introduced in the HMF equations. Specifically, there does not exist solid basis to couple the size of each subpopulation with its number of connections in the mobility network. For this reason, Belik et al.[9,57] propose an alternative model which abandons the statistical equivalence of all patches within the same degree class k. In this model, also in the SIR domain, the evolution of the infected and susceptible individuals associated with each patch k and located at each patch n, I_n^k and S_n^k respectively, is given by

$$\partial_t I_n^k = \frac{\lambda}{N_n} S_n^k \sum_m I_n^m - \mu I_n^k + \sum_m \left(\omega_{mn}^k I_m^k - \omega_{nm}^k I_n^k\right) \tag{9}$$

$$\partial_t S_n^k = -\frac{\lambda}{N_n} S_n^k \sum_m I_n^m + \sum_m \left(\omega_{mn}^k S_m^k - \omega_{nm}^k S_n^k\right) \tag{10}$$

where ω_{nm}^k encodes the diffusion rate from patch n to patch m for individuals with residence in k. In this general framework, strictly commuting patterns are therefore included by considering $\omega_{nm}^k = \delta_n^k \omega_{nm}$, being δ_n^k the Kronecker delta. Armed with these equations, the authors study the propagation of diseases across simple synthetic configurations, finding that outbreaks in structured lattices can be characterized as continuous waves propagating across a media with a well-defined front propagation. In this model, the authors also observe the acceleration of epidemic outbreaks driven by longer typical times associated with the trips.

The model proposed in refs. [9, 57] constitutes the first step toward understanding the microscopic processes behind the complex interplay between recurrent mobility and epidemic spreading. Nonetheless, it still contains some theoretical limitations. Specifically, the model assumes a constant rate governing contagion events across the entire metapopulation, which implies that the number of interactions made by one agent is constant and independent of the place in which the individual is located. This limits the application of the model to some scenarios where the attributes of a node or patch determine its vulnerability for disease spreading; for example, the model cannot capture the recently reported evidence about the positive correlation existing between population density and the number of COVID-19 cases in different countries.[58–60]

4. MIR Model

Following the aforementioned works, the authors in refs. [61, 62] propose the MIR model. Unlike previous formalisms, this model constitutes a discrete-time approach where each time step is composed by three stages, which are schematically depicted in **Figure 3**:

1. Movement: At the beginning of the day, the population decide whether or not to move with probability p. This probability acts as a control parameter which allows activating or deactivating mobility at convenience. If an individual decides to move, he or she decides the destination according to the OD matrix $\mathbf{R}$ whose elements R_{ij} encode the weights of the links connecting patches i and j in the metapopulation.
2. Interaction: Once all the movements have been completed, the reaction phase starts and individuals interact, changing their epidemiological state accordingly. Note that this phase aims at capturing the contacts made at the workplace, school, etc. Formally, the authors introduce a mean-field assumption within each patch, which implies that all the individuals placed at the same location make the same number of contacts. As stated above, this number of contacts is not constant across the metapopulation but is usually a function f of the attributes of the patches.
3. Return: Finally, to reflect the recurrent nature of commuting mobility, all the individuals return to the associated residential patches. Note that this model gets rid of the dwelling times, whose effect will be later analyzed in this review.

The iteration of these three stages simulates the daily dynamics of contagious diseases in a given metapopulation. Note that this framework presents several drawbacks. First, the time-discrete equations do not account for the continuous nature of human mobility and neglect the influence of more complex mobility patterns beyond strictly back-and-forth displacements. This assumption simplifies the equations of the model and is partially supported by statistics[63] reporting that commuting patterns represent around 30–50% of the daily movements. Second, the contribution of the interactions made with the household members after the return stage is neglected. In that respect, Granell et al. propose in ref. [64] the natural extension of the model to overcome this limitation by incorporating two interactions stages corresponding to both contagions occurring outside and inside the household. The qualitative findings about the interplay between mobility and epidemics are consistent for both formalisms so, for the sake of simplicity, we focus on the MIR model to explain them.

4.1. Model Equations

As this review gravitates around the MIR model, we now introduce the set of Markovian equations determining the evolution of epidemics according to this model. From a structural point of view, the model considers a metapopulation with N_p patches and assume that each patch i is populated by n_i residents, whereas the flows between the different patches are captured in the OD matrix $\mathbf{R}$. Under these conditions, the course of a SIS disease is entirely characterized by the time evolution of the fraction of

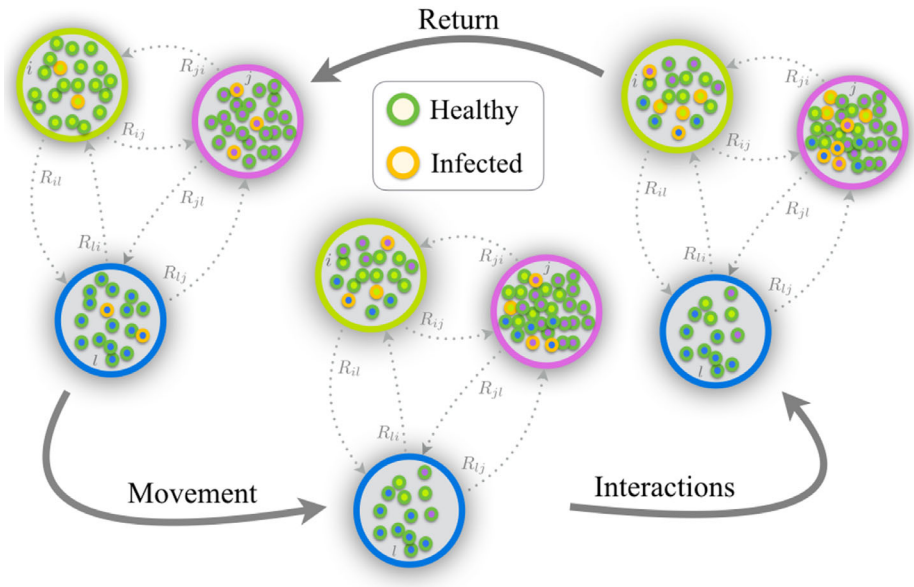

Figure 3. Schematic representation of one time step of the movement-interaction-return (MIR) metapopulation model. The metapopulation is composed of $N_P = 3$ patches. At the movement stage, some of the local agents decide to move to the other patches according to the mobility probability p and the mobility patterns encoded in matrix **R**. After moving, the agents interact in a well-mixed way and change their epidemic state (healthy or infected) according to a SIS model. Finally, they come back to their home patches and a new time step starts. Reproduced with permission.[62] Copyright 2018, APS.

individuals living in each patch i in the infected state, denoted in the following by ρ_i. This time evolution is given by

$$\rho_i(t+1) = (1-\mu)\rho_i(t) + \left[1-\rho_i(t)\right]\Pi_i(t) \tag{11}$$

The first term in the r.h.s of Equation (11) contains those infected individuals associated with patch i not recovering at time t. The second term in the r.h.s of Equation (11) reflects the contagions of the susceptible population.

Note that, although the review focuses on the SIS model, the MIR model can be extended to account for more complex compartmental schemes. For instance, in the case of the SIR model, the dynamics is completely characterized by the following system of equations

$$\rho_i(t+1) = (1-\mu)\rho_i(t) + \left[1-\rho_i(t)-r_i(t)\right]\Pi_i(t) \tag{12}$$

$$r_i(t+1) = r_i(t) + \mu\rho_i(t) \tag{13}$$

where $r_i(t)$ denotes the fraction of individuals associated with patch i in the recovered state at time t.

Regardless of the compartmental scheme, a central object of the MIR model is $\Pi_i(t)$, which represents the probability that a susceptible agent living inside i contracts the disease. Taking into account the microscopic rules of the MIR model, this probability is given by

$$\Pi_i(t) = (1-p)P_i(t) + p\sum_{j=1}^{N_P} R_{ij}P_j(t) \tag{14}$$

where the first term encodes the contagions in the residential patch and the second one corresponds to the contagions occurring when one individual from patch i moves across the metapopulation. Therefore, $P_i(t)$ corresponds to the probability that a susceptible individual, regardless of his or her residential patch, contracts the disease inside patch i. Given the well-mixing hypothesis introduced in the model, this probability is

$$P_i(t) = 1 - \left[1 - \lambda\frac{\tilde{I}_i(t)}{\tilde{n}_i}\right]^{f_i} \tag{15}$$

where $\tilde{n}_i$ represents the effective population of patch i, that is, the number of individuals placed at patch i after the movement stage and $\tilde{I}_i(t)$ is the effective number of infected individuals inside patch i at time t. Taking into account the demographic distribution of the population and the mobility patterns, both quantities are easily computed as

$$\tilde{n}_i = \sum_{j=1}^{N_P} n_{j\to i} = \sum_{j=1}^{N_P} n_j\left[(1-p)\delta_{ij} + pR_{ji}\right] \tag{16}$$

$$\tilde{I}_i(t) = \sum_{j=1}^{N_P} I_{j\to i} = \sum_{j=1}^{N_P} n_j\rho_j(t)\left[(1-p)\delta_{ij} + pR_{ji}\right] \tag{17}$$

where $n_{j\to i}$ and $I_{j\to i}$ represent the total number of residents and the number of infected individuals moving from patch j to patch i respectively.

4.2. Validation on Synthetic Networks

Equations (11)–(17) form a closed set of equations, whose iteration allows for characterizing the spatio-temporal spread of contagious diseases. For the sake of simplicity, the authors

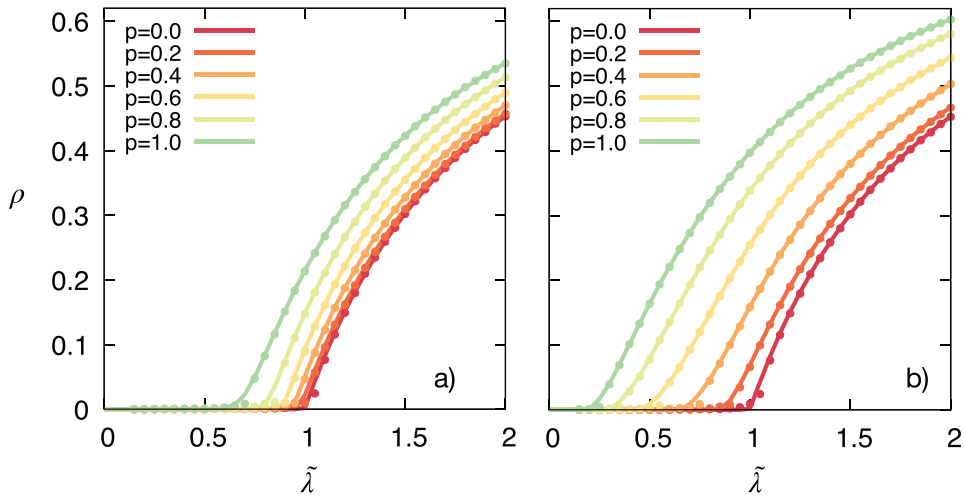

Figure 4. Evolution of the epidemic size ρ as a function of the rescaled infectivity $\tilde{\lambda}$ and the mobility p (color code). The rescaled infectivity is obtained by dividing the actual infectivity λ by the expected threshold for an isolated metapopulation, that is, $\tilde{\lambda} = \lambda n/\mu$. a) The metapopulation is an ER network. b) The curves for a BA network. both with $N_P = 10^3$ patches, $\langle k \rangle \approx 4$ and random weights assigned to the links. In both panels, the solid lines represent the numerical results obtained by iterating Equations (11)–(17) whereas points show the average of the epidemic size values obtained from 50 Monte Carlo simulations. The recovery probability is set to $\mu = 0.2$. Reproduced with permission.[62] Copyright 2018, APS.

first assume that interaction processes take place all-to-all within each patch, implying that $f_i = \tilde{n}_i$. In that case, a more accurate expression for the probability of contracting a disease inside a patch, P_i, can be proposed by leveraging the statistical independence of the different patches, implying the existence of different infection levels across the metapopulation.[61] Namely

$$P_i(t) = 1 - \prod_{j=1}^{N_P} \left(1 - \lambda \rho_j\right)^{n_{j\to i}} \tag{18}$$

To illustrate the validity the equations, the model is run in synthetic networks with $N_P = 10^3$ patches, which are homogeneously populated by $n = 5000$, yielding $N = 5 \times 10^6$ individuals. Moreover, to unravel the role of heterogeneities in terms of spatial connections, two different undirected and unweighted mobility networks are generated according to both the Erdös–Rényi (ER)[65] and the Barabási–Albert (BA)[66] models. The global extent of the outbreak is quantified by the epidemic size ρ, defined as the total fraction of individuals in the infectious state when the disease reaches the stationary state. We start by infecting 1% of the population of each node and let the system evolves until no variations are observed in the number of infected individuals. According to the variables of the MIR model, the epidemic size ρ is computed as

$$\rho = \frac{\sum_{i=1}^{N_P} n_i \rho_i(\infty)}{\sum_{i=1}^{N_P} n_i} \tag{19}$$

In **Figure 4** the epidemic size ρ is represented as a function of the rescaled infectivity $\tilde{\lambda}$ for several mobility scenarios in the ER (a) and BA (b) metapopulations. The rescaled infectivity is computed by dividing the infectivity λ by the expected threshold for a SIS model in a well-mixed population of size n, so $\tilde{\lambda} = \lambda n/\mu$. There, it becomes clear that the equations of the MIR model are able to capture the results from microscopic Monte Carlo simulations. Regarding the role of human movements, promoting mobility from the static case ($p = 0$) to the fully active population ($p = 1$), leads to an increase in the epidemic size, pinpointing that mobility accelerates epidemic diffusion as suggested in previous works. This acceleration gains relevance in case of heterogeneous mobility networks, for heterogeneity favors the gathering of a higher number of individuals inside the most connected areas. This result is aligned with previous findings made in the theoretical frameworks relying on HMF approaches described in Section 3.[55]

4.3. Epidemic Threshold

The analysis made in synthetic metapopulations for the MIR model reveals that the impact of mobility is highly influenced by the structural properties of the underlying metapopulation. To characterize analytically the interplay between mobility and epidemics, the authors in ref. [61] linearize the Markovian equations governing the evolution of the dynamics and find a closed expression for the epidemic threshold λ_c, delimiting the minimum infectivity required to observe an endemic equilibrium. In particular, they find that

$$\lambda_c = \frac{\mu}{\Lambda_{\max}(\mathbf{M})} \tag{20}$$

where the elements of the matrix $\mathbf{M}$ are given by:

$$M_{ij} = n_j \left[\delta_{ij}(1-p)^2 \frac{f_j}{\tilde{n}_j} + p(1-p)\left(\frac{R_{ij} f_j}{\tilde{n}_j} + \frac{R_{ji} f_i}{\tilde{n}_i} \right) + p^2 \sum_{l=1}^{N_P} \frac{R_{il} R_{jl} f_l}{\tilde{n}_l} \right] \tag{21}$$

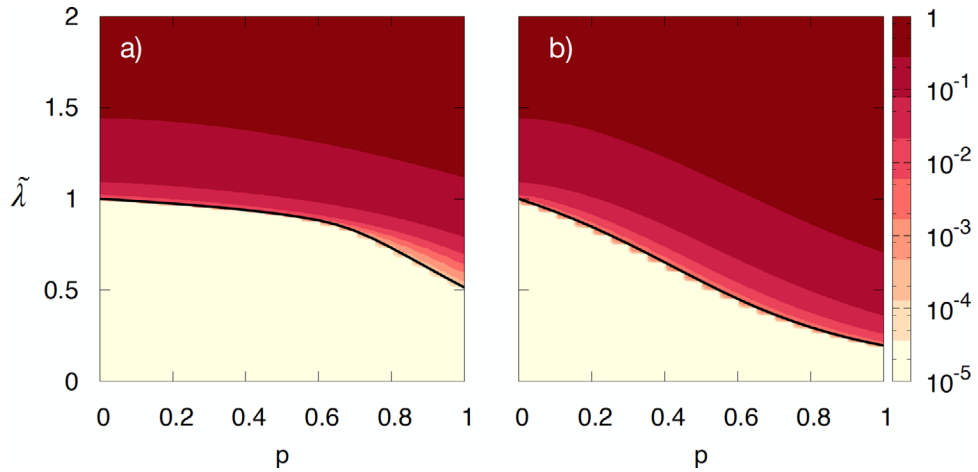

Figure 5. Epidemic size ρ obtained by the numerical iteration of Equation (11)–(17) (color code) as a function of the mobility p and the rescaled infectivity $\tilde{\lambda}$. The black solid lines show the analytical estimation for the epidemic threshold computed by Equation (20) for the ER (a) and the BA (metapopulations). Reproduced with permission.[62] Copyright 2018, APS.

Note that this expression resembles the epidemic threshold derived for SIS dynamics on contact networks[67] but here, rather than the adjacency matrix **A**, a more complex matrix **M** governs the interactions of the population. Specifically, the elements M_{ij} correspond to the expected number of interactions made by one individual from patch i with the population residing in patch j. In particular, the first term corresponds to those contacts taking place between individuals from the same patch and not moving. The second (third) term encodes the contacts made where the agent from i (j) moves to patch j (i) and interacts with the population remaining there. Finally, the fourth term contains all the interactions taking place in a third node different from the patches associated with the agents in contact.

Figure 5 shows the dependence of the epidemic size on the mobility p and the infectivity λ along with the estimation of the epidemic threshold computed by Equation (20). There we observe that the analytical expression found in ref. [61] for the epidemic threshold captures the phase transition between the disease-free state and the emergence of a stable endemic regime in both synthetic metapopulations and the higher vulnerability induced by heterogeneous mobility networks.

4.4. Real Metapopulations

One of the main advantages of the MIR model with respect to the aforementioned works relying on HMF approaches is the fact that no assumptions are made concerning the statistical equivalence of the different patches. Therefore, data about the demographic distribution and the mobility of the population can be readily incorporated into the equations of the MIR model to study the relevance of commuting for disease spreading in real cities.

Different alternatives have been proposed in the literature to capture the mobility patterns of the populations such as census surveys[68,69] or the location history inferred from call detailed records,[70,71] the activity on social platforms,[15,72] or mobile-phone devices.[73,74] Leveraging the information provided by extensive census surveys carried out to the Colombian population, the authors in refs. [61, 62] apply the MIR model to characterize the spread of SIS diseases over the cities of Santiago de Cali and Medellín. The resulting metapopulations, with $N_P = 22$ patches and $N_P = 413$ patches in Cali and Medellin respectively, corresponding to different administrative divisions, are schematized in **Figure 6**a,b.

Figure 6c,d represent the epidemic size ρ as a function of the rescaled infectivity $\tilde{\lambda}$ and the degree of mobility p for both metapopulations, along with the estimation for the epidemic threshold $\tilde{\lambda}_c$. Remarkably, increasing mobility in real heterogeneous metapopulations has a counterintuitive effect on the dynamics. Namely, rather than boosting epidemic spreading as observed in synthetic metapopulations, promoting population movements might be beneficial to contain an ongoing outbreak. Namely, in both cases the initial increase of the threshold for both cities implies that mobility prevents the endemic equilibrium from being reached, therefore hindering the spread of diseases.

It is worth noticing that the qualitative dependence of the threshold on the mobility for both cities is different. While for the city of Medellín increasing mobility always makes the city less prone to epidemic outbreaks, in the case of Cali the beneficial effect of such intervention is reversed in the regime of high mobility, leading to the expected acceleration of the diffusion of epidemics. Summarizing the results presented thus far, three different types of metapopulations according to the dependence of the epidemic threshold on the mobility of the population, p, are observed. In what follows, we denote these categories by Types I, II, and III respectively.

- Type I: In these metapopulations, increasing mobility always fosters epidemic spreading, which is reflected in a monotonic reduction of the epidemic threshold $\tilde{\lambda}_c$ when increasing the mobility p. Synthetic metapopulations whose nodes are uniformly populated fall into this category.
- Type II: In this case, the epidemic threshold shows a non-trivial behavior with the mobility. For small p values, the epidemic threshold increases with the mobility, giving rise to

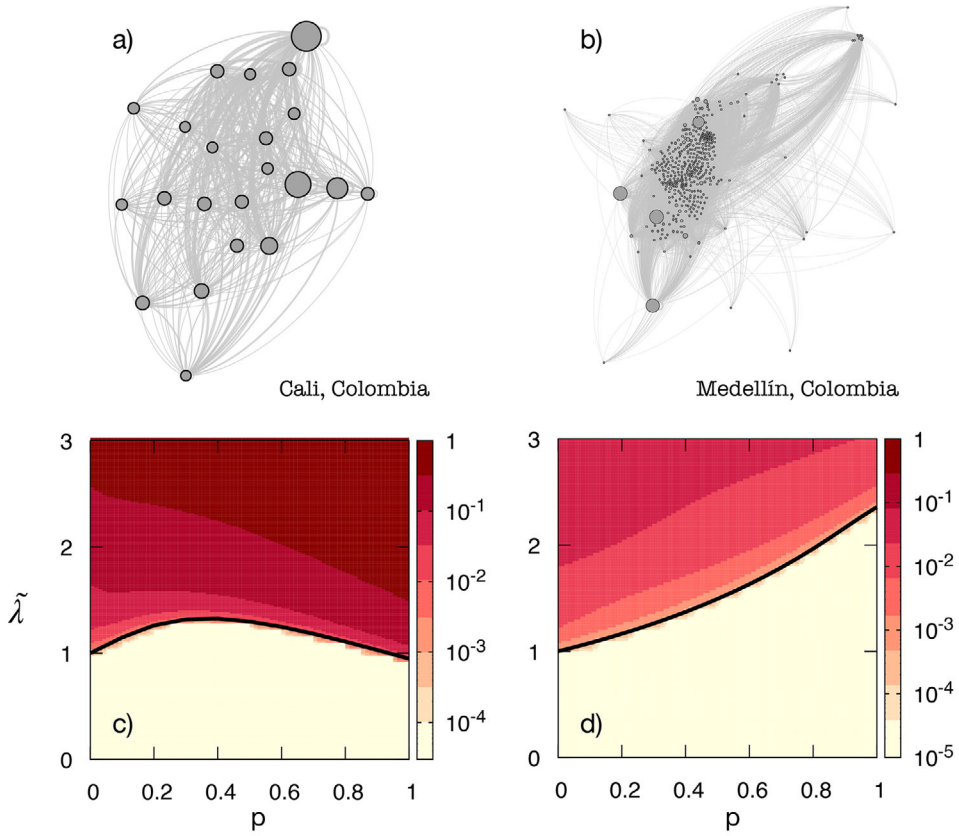

Figure 6. Spread of diseases across real metapopulations. a,b) S schematic representation of the metapopulations of the cities of Cali (a) and Medellín (b) in Colombia. In both panels, the size of each patch is proportional to its population, whereas the flows are extracted from census surveys (see text for more details). c,d) Epidemic size ρ obtained by the numerical iteration of Equations (11)–(17) (color code) as a function of the mobility p and the rescaled infectivity $\tilde{\lambda}$ for the city of Cali and Medellín respectively. The black solid lines show the analytical estimation for the epidemic threshold computed by Equation (20) for each case. In all panels, the recovery probability is set to $\mu = 0.2$. (a) and (c) adapted with permission.[61] Copyright 2018, Springer and (b) and (d) reproduced with permission.[62] Copyright 2018, APS.

the so-called epidemic detriment. This trend is maintained up to a given value of the mobility, p^*, for which the epidemic threshold reaches its peak. Afterward, the impact of mobility is reversed and promoting movements boosts epidemic spreading and hence decreases the epidemic threshold. The city of Cali in Colombia constitutes one example of a Type II metapopulation.

- Type III: Finally, there are other cases, like the city of Medellín in Colombia, where the epidemic detriment appears consistently from the static case $p = 0$ to the case in which the entire population moves according to the mobility network $p = 1$.

Figure 7a depicts the dependence of the threshold on the mobility for the three different types of cities. To get more empirical evidence on the complex interplay between mobility and epidemics, Hazarie et al.[75] extract the p^* value for 163 cities distributed across four countries: United States, Italy, Australia and South Africa. Unlike the networks above described for Colombian cities, the mobility patterns in this study are extracted from the Google COVID-19 Aggregated Mobility Research Dataset, which contains anonymized mobility flows aggregated over users who have turned on the Location History setting, which is off by default. Regarding the function governing contacts, the authors abandon the all-to-all interaction scheme and make the number of contacts inside a given patch i dependent on its population density. Mathematically, they assume that $f_i = \tilde{n}_i / a_i$, being $\tilde{n}_i$ defined by Equation (16) and a_i the area of patch i. Figure 7b contains the histogram of the p^* values, finding 109 Type II ($p^* < 1$) and 54 Type III ($p^* = 1$) metapopulations.

5. Origin of the Epidemic Detriment

In what follows, we detail the mathematical and physical arguments proposed to justify the emergence of the epidemic detriment and understand the complex interplay existing between recurrent mobility and epidemics.

5.1. Perturbative Expansion

Mathematically, Gómez–Gardeñes et al.[61] explore the roots behind the epidemic detriment by performing a perturbation analysis of the matrix $\mathbf{M}$.[76] Focusing on the case $f_i = \tilde{n}_i$, after rearranging the terms in Equation (21), the elements M_{ij} read as

$$M_{ij} = M_{ij}^0 + pM_{ij}^1 + p^2 M_{ij}^2 \tag{22}$$

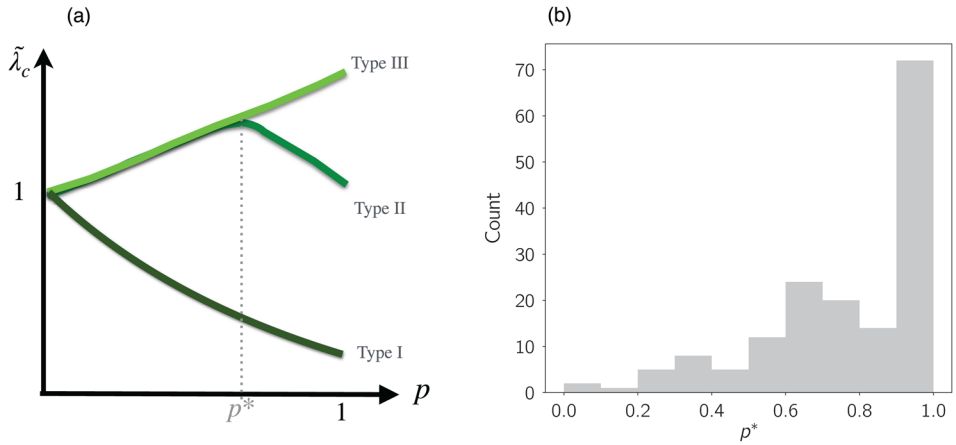

Figure 7. Rescaled epidemic threshold $\tilde{\lambda}$ as a function of the mobility p for the three different qualitative behaviors observed so far. Type I cities show a continuous reduction of the threshold while increasing p, so mobility boosts epidemic spreading. The epidemic detriment, for which increasing mobility hinders the spread of diseases, is nonmonotonic for Type II cities, since it appears for small p values and vanishes after the peak located at $p = p^*$, and monotonic for Type III cities. b) Histogram of the p^* values extracted from the dependence of the rescaled epidemic threshold on the mobility $\tilde{\lambda}_c(p)$ for each of the 163 cities analyzed in ref. [75]. Reproduced with permission.[75] Copyright 2021, Springer.

with

$$M^0_{ij} = n_j \delta_{ij} \tag{23}$$

$$M^1_{ij} = n_j (R_{ij} + R_{ji} - 2\delta_{ij}) \tag{24}$$

$$M^2_{ij} = n_j \left[(\mathbf{R} \cdot \mathbf{R}^{\mathrm{T}})_{ij} - R_{ij} - R_{ji} + \delta_{ij} \right] \tag{25}$$

Based on perturbation theory, the leading eigenvalue of matrix $\mathbf{M}$ can be approximated by

$$\Lambda_{\max}(\mathbf{M}) = \Lambda_{\max}(\mathbf{M^0}) + p\Lambda^1 + p^2\Lambda^2 \tag{26}$$

with

$$\Lambda^1 = \langle v^0_{\max} | \mathbf{M^1} | v^0_{\max} \rangle \tag{27}$$

$$\Lambda^2 = \sum_{j \neq \max} \frac{\langle v^0_j | \mathbf{M^1} | v^0_{\max} \rangle \langle v^0_{\max} | \mathbf{M^1} | v^0_j \rangle}{\Lambda_{\max} - \Lambda_j} + \langle | v^0_{\max} | \mathbf{M^2} | v^0_{\max} \rangle \tag{28}$$

In both expressions, $\{v^0_j\}$ represents the eigenvector basis and, in particular, $v^0_{\max}$ represents the eigenvector associated with the leading eigenvalue of the matrix $\mathbf{M^0}$. Taking into account that the matrix $\mathbf{M^0}$ is diagonal, the eigenvalues correspond to the population of each patch and the eigenvector basis is the canonical basis, which simplifies the calculus of the different corrections. Assuming that the outbreak is localized for $p = 0$ inside the patch i, these corrections read as

$$\Lambda^0 = n_i \tag{29}$$

$$\Lambda^1 = 2n_i(R_{ii} - 1) \tag{30}$$

$$\Lambda^2 = n_i \left\{ (1 - R_{ii})^2 + \sum_{j \neq i} \left[\frac{n_j (R_{ij} + R_{ji})^2}{n_i - n_j} + R^2_{ij} \right] \right\} \tag{31}$$

Note that the linear correction is always negative, ensuring that for low enough p values, the leading eigenvalue of the critical matrix $\mathbf{M}$ decreases, which leads to the increase of the epidemic threshold responsible for the epidemic detriment. Interestingly, the second-order correction is always positive, thus explaining the nonmonotonic behavior observed for the epidemic threshold as the result of the trade-off between these two opposite contributions. Finally, by decreasing the heterogeneity of the population distribution, the second term becomes dominant, thus shrinking the epidemic detriment regime, which finally vanishes for homogeneous populations, as observed in the synthetic metapopulations.

5.2. Star-Like Metapopulation Structure

To explain heuristically the mechanisms responsible for the emergence of the epidemic detriment, Gómez–Gardeñes et al.[61] make use of a synthetic metapopulation, the star-like city. Star networks are simple graphs composed of a central node, usually referred to as hub, which is linked to a set of peripheral nodes, the so-called leaves. The main advantage of these simple configurations is the statistical equivalence of all the leaves, which greatly simplifies the theoretical analysis of different dynamics. For example, the use of star networks has been crucial to analytically characterize the nature of different phenomena such as the onset of SIS diseases,[77,78] the microscopic origin of the explosive synchronization,[79] or the oscillations in chemical reaction-diffusion processes.[80]

Figure 8a depicts schematically the structure of the star-like city. Note that the metapopulation is fully characterized by four parameters:

1. $n_{\max}$: Number of residents inside the hub so that $n_{\mathrm{h}} = n_{\max}$.
2. κ: Number of leaves surrounding the hub. Note that the flows from the central node to the periphery are uniformly distributed so that $R_{\mathrm{hl}} = 1/\kappa$.

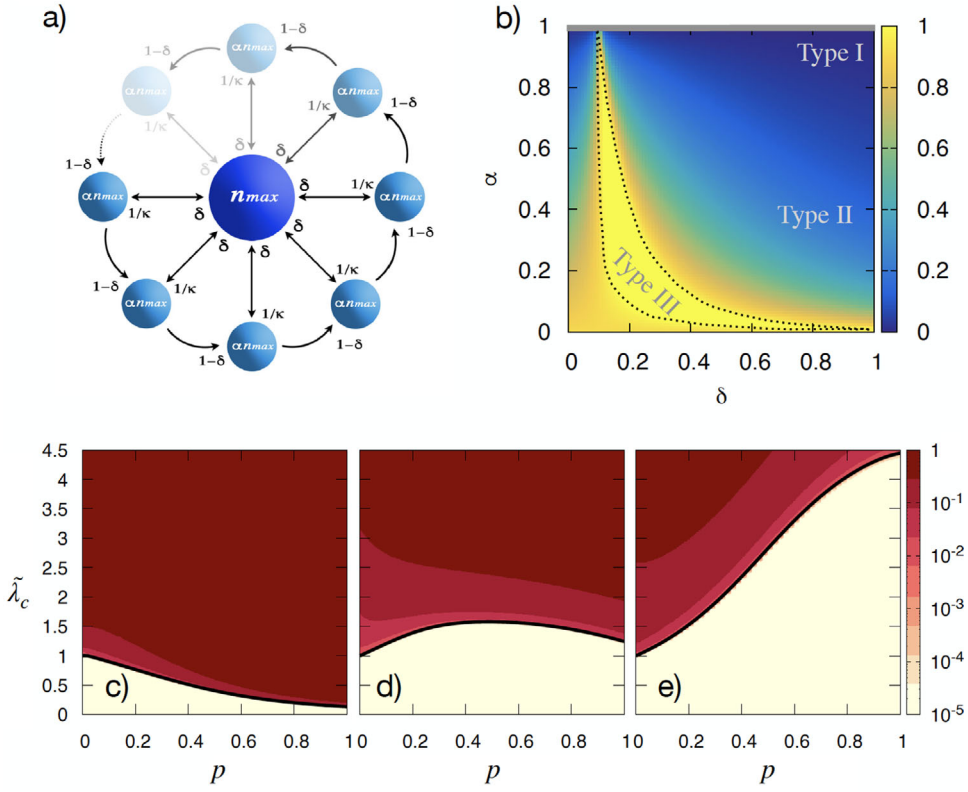

Figure 8. a) Schematic representation of the star-like metapopulation. The relevant parameters are the population of the hub n_{max}, the population asymmetry α, the number of leaves κ and the flow from leaves to the hub δ (see text for details). b) p^* (color code) as a function of (α, δ) for a star-like metapopulation with $\kappa = 10$ leaves. c–e) Epidemic size ρ (color code) as a function of the rescaled infectivity $\tilde{\lambda}$ and the mobility p. The solid black line depicts the analytical estimation for the rescaled epidemic threshold provided by Equation (38). Reproduced with permission.[61] Copyright 2018, Springer.

3. α: Population asymmetry between the hub and the leaves. In this sense, each leaf is populated by $n_l = \alpha n_{max}$ agents with $\alpha \in [0, 1]$.
4. δ: Fraction of the flows departing from the leaves which end in the hub, that is, $R_{lh} = \delta$. The remaining fraction of the moving population goes to the next leaf in the counterclockwise direction so that $R_{l,l+1} = 1 - \delta$.

Mathematically, the statistical equivalence of the leaves allows reducing the dimensionality of the system from N_p to 2 equations, governing the evolution of the disease inside the hub and a generic leaf respectively. Denoting the hub and the leaves by the subscripts h and l, respectively, and focusing on the all-to-all interaction scheme, the elements of the critical matrix $\mathbf{M}$ are given by

$$M_{hh} = n_{max}\left[(1-p)^2 + p^2/\kappa\right] \tag{32}$$

$$M_{hl} = \kappa\alpha n_{max}\left[p(1-p)(1/\kappa+\delta) + p^2(1-\delta)/\kappa\right] \tag{33}$$

$$M_{lh} = n_{max}\left[p(1-p)(1/\kappa+\delta) + p^2(1-\delta)/\kappa\right] \tag{34}$$

$$M_{ll} = \alpha n_{max}\left\{(1-p)^2 + 2p(1-p)(1-\delta) + p^2\left[\kappa\delta^2 + (1-\delta)^2\right]\right\}. \tag{35}$$

As a result of the dimensionality reduction, the matrix $\mathbf{M}$ is a 2×2 matrix, whose leading eigenvalue can be computed analytically. This allows obtaining a simple expression for the epidemic threshold, which now reads as

$$\lambda_c = \frac{\mu}{\Lambda_{max}(\mathbf{M})} \tag{36}$$

with

$$\Lambda_{max}(\mathbf{M}) = \frac{\mathrm{tr}(\mathbf{M}) + \sqrt{\mathrm{tr}(\mathbf{M})^2 - 4\det\mathbf{M}}}{2} \tag{37}$$

The expression for the epidemic threshold depends on five parameters, the four characterizing the properties of the underlying metapopulation and the recovery rate μ. To focus on the effect of the mobility, the authors focus on the rescaled epidemic threshold

$$\tilde{\lambda}_c = \frac{\lambda_c}{\lambda_c(p=0)} = \frac{n_{max}}{\Lambda_{max}(\mathbf{M})} \tag{38}$$

Note that all the elements of the matrix $\mathbf{M}$ depend linearly on the population of the hub n_{max}, which makes the rescaled epidemic threshold independent of this parameter. In plain words,

the qualitative impact of the mobility is not a variable of the overall number of agents in the metapopulation but is only influenced by the population asymmetries governed by α and the features of the mobility network determined by (κ, δ).

The star-like configuration retrieves the three different types of cities described above. Figure 8b represents the value of p^* as a function of (α, δ) when fixing $\kappa = 10$ leaves. There we observe how Type I cities ($p^* \to 0$) are restricted to the areas of the parameters' space with $\alpha \simeq 1$ and therefore to metapopulations with negligible population asymmetries, as suggested by the perturbation analysis. The rest of the phase diagram shows a non-trivial boundary between Type II and Type III cities. In particular, most of the possible configurations correspond to Type II cities whereas Type III cities are associated with a very specific region of the parameters' space. For the sake of completeness, Figure 8c–e shows the epidemic diagrams for three different combinations of (α, δ), identifying the three possible types of cities.

To connect the dots between the structural features of the metapopulation and the observed p^* value, it is worth recalling that in the MIR model the number of contacts each individual makes is an extensive variable which depends on the attributes of the place where she/he is located. In particular, under the all-to-all interactions scheme, this number of contacts matches the effective population of the different patches. Intuitively, one plausible explanation for the epidemic detriment would be that mobility tends to homogenize the underlying population distribution, thus reducing the number of individuals interacting inside the most vulnerable node and, therefore, requiring a higher infectivity to observe a macroscopic outbreak. In the star-like metapopulation, the effective populations of both the hub and the generic leaf read as

$$\tilde{n}_h = n_{\max}\left[(1-p) + \alpha\kappa p\delta\right] \tag{39}$$

$$\tilde{n}_l = n_{\max}\left[\alpha(1-p\delta) + p/\kappa\right] \tag{40}$$

Equating both equations, we can estimate the value at which the effective population inside the leaf becomes higher than the one gathered in the hub, denoted in what follows by p^*_{heur}, yielding

$$p^*_{\text{heur}} = \frac{\kappa(1-\alpha)}{(\kappa+1)(1-\delta\alpha\kappa)} \tag{41}$$

Figure 9a shows the dependence of the latter indicator as a function of the population asymmetry α and the flows from leaves to the hub, governed by δ. Interestingly, two clearly differentiated regions appear in this figure:

- $k\delta\alpha \leq 1$: In this region of the parameters' space, mobility tends to reduce the population gathered inside the hub and increase the population in the leaves, as shown in Figure 9b. Remarkably, the value predicted relying on the homogenization of the population is able to capture very accurately the actual value of p^* represented in Figure 8b.
- $k\delta\alpha > 1$: In this case, the value derived for p^*_{heur} is always negative, for the distribution of population is no longer homogenizing. Instead mobility tends to accumulate individuals inside the hub at the expense of emptying the leaves, as captured in Figure 9c. Therefore, the epidemic detriment observed in Figure 8 and universally predicted by the perturbation analysis cannot be justified based on the redistribution of the population.

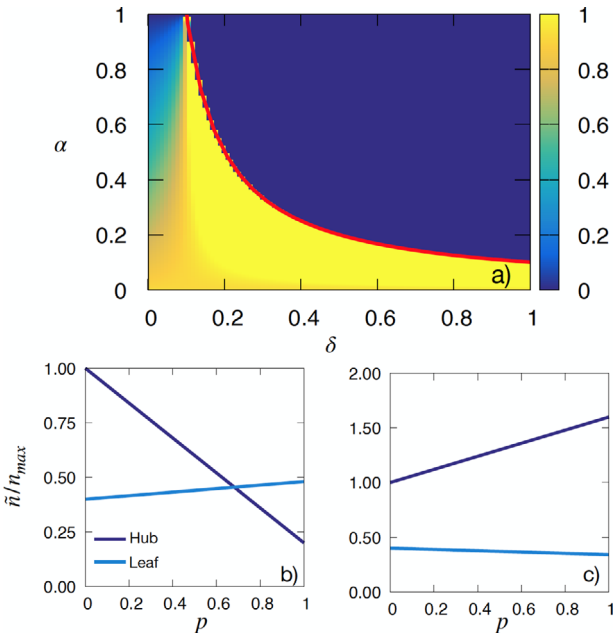

Figure 9. a) Value of the heuristic estimation for the position of the peak of the epidemic threshold p^*_{heur} (color code) as a function of the population asymmetry α and the parameter δ governing the flow from the leaves to the hub. The solid red line depicts the function $\alpha = 1/(\kappa\delta)$, which delimits the region where macroscopic arguments work to explain the epidemic detriment (see text for details). b–c) Dependence of the effective population interacting inside the hub $\tilde{n}_h$ and the leaves $\tilde{n}_l$ on the mobility p for two star-like metapopulations with $(\alpha, \delta) = (0.4, 0.05)$ (b) and $(\alpha, \delta) = (0.4, 0.4)$ (c) respectively. In all the cases, the number of leaves is $\kappa = 10$.

The failure of macroscopic arguments based on the sizes of the interacting populations suggests that the epidemic detriment, and more in general the interplay between recurrent mobility and epidemics, are driven by processes taking place across microscopic/mesoscopic scales. The crucial role of these processes in the emergence of the epidemic detriment is supported by two extensions of the MIR model which overcome some of its theoretical limitations.

5.3. MIR Model with Tunable Return Times

First, Soriano-Paños et al.[81] introduce a new time scale in the model, denoted in what follows by τ, which encodes the number of epidemic time steps that agents spend outside their residence before returning to them. This time scale retrieves the dwelling times introduced in the HMF approaches explained in Section 3[35,55,56,82,83] and leads to important variations of the epidemic trajectories.

The asymmetry between the time scales involved in the contagions and the movements provokes that the initial population of each patch at each time step is not only composed of residents but also contains visitors not returning to their residential patch.

Therefore, the different stages of the MIR model must be adapted to accommodate the new time scale. In particular:

1. Movement: At the beginning of each time step, the residents in one patch decide whether to leave it with a probability p or remain there with probability $1-p$. To respect the commuting nature of human movements and the new time scale, visitors in one patch are not allowed to move. Mathematically, this can be represented as a third-order tensor $\mathcal{R}$, whose elements $\mathcal{R}^i_{jk}$ denote the probability that a resident inside i moves from j to k. Note that, in general, the tensor $\mathcal{R}$ allows for accommodating a wide variety of mobility schemes ranging from higher-order paths[84] to random walker dynamics. In our case of interest, the assumptions described above lead to

$$\mathcal{R}^i_{jk} = \delta^i_j R_{jk} + (1-\delta^i_j)\delta_{jk} \tag{42}$$

   where $\mathbf{R}$ is the OD matrix used in the original MIR model.
2. Interaction: This stage remains as in the original MIR model. In this case, both residents and visitors are indistinguishable and make the same number of contacts depending on the attributes of the place where they are located after the movement stage. In each contact between susceptible and infected individuals, the first one contracts the disease with probability λ. Likewise, infected individuals can overcome the disease with a given probability μ.
3. Return: Finally, visitors decide whether returning home with probability τ^{-1} or staying at their destination with probability $1-\tau^{-1}$.

After deriving the corresponding Markovian equations, the authors prove that the epidemic threshold in presence of tunable return times is given by

$$\lambda_c = \frac{1}{\Lambda_{\max}(\mathbf{F}\mathbf{V}^{-1})} \tag{43}$$

with

$$\begin{aligned} F^{il}_{jm} = \delta^i_j \Bigg\{ & n^i_i\left[1-p'_i\right]\left[\delta^{il}\delta^i_m\left(1-p'_l\right)+\left(1-\delta^{il}\right)\left[pR_{li}\delta^l_m+\delta_{mi}\right]\right] \\ & + \tau^{-1}\left(1-\delta^i_m\right)\delta^l_m\left(R_{im}+n^i_m\right)\left(1-p(1-R_{lm})\right) \\ & + \tau^{-1}\delta^l_m\sum_{o=1}^{N_p}\left(1-\delta^i_o\right)\left(pR_{io}n^i_i+n^i_o\right)pR_{lo} \\ & + \tau^{-1}\left(1-\delta^i_m\right)\left(1-\delta^l_m\right)\left(pR_{im}n^i_i+n^i_m\right)\Bigg\} \\ & + (1-\delta^i_j)(1-\tau^{-1})(pR_{ij}n^i_i+n^i_j) \\ & \left[\delta^l_j\delta^l_m(1-p'_k)+(1-\delta^l_m)(pR_{lj}\delta^l_m+\delta_{mj})\right] \end{aligned} \tag{44}$$

and

$$\begin{aligned} V^{il}_{jm} = {} & \delta^i_j\delta^{li}\left[\delta^i_m\left(\mu+p'_i(1-\mu)(1-\tau^{-1})\right)-(1-\delta^i_m)(1-\mu)\tau^{-1}\right] \\ & +(1-\delta^i_j)\left[\delta^{il}\delta_{jm}(\mu+\tau^{-1}(1-\mu)-\delta^l_m(1-\mu)(1-\tau^{-1})pR_{lm}\right] \end{aligned} \tag{45}$$

The elements F^{il}_{jm} encode the contagion processes from those individuals associated with the residence i and the destination j to those living inside the patch l and commuting to m, whereas the elements V^{il}_{jm} constitute the redistribution of the infectious population across the system. To quantify the relevance of the new time scale, let us fix $\alpha=\delta=0.4$ and $\kappa=10$ leaves. It is worth recalling that macroscopic arguments based on the redistribution of the population cannot justify the emergence of the detriment in such configuration, for mobility tends to accumulate agents inside the hub. **Figure 10**a contains the epidemic threshold $\tilde{\lambda}_c$ as a function of the mobility p and the trip duration τ. There a striking result shows up: the epidemic detriment vanishes when increasing the permanence times at the destination. Specifically, increasing τ (reducing τ^{-1}) always decreases the value of p^* from the one observed in the original MIR model to $p^*=0$, at which the epidemic detriment is no longer observed. Apart from the anticipation of the peak p^*, the effect of mobility is boosted as one increases the new time scale introduced, which is reflected in the higher slope of the threshold for small p values.

Macroscopically, both phenomena suggest that increasing the permanence times comprises the curves of the original MIR model and introduces an effective mobility higher than the actual mobility p. Nonetheless, this argument fails in capturing the behavior of the system for $p=1$. Note that the effective population of the hub in this case reads

$$\tilde{n}_h\Big|_{p=1} = \alpha\kappa\delta \tag{46}$$

which is independent of the permanence time. However, the epidemic threshold is significantly reduced when extending the trip duration; this is the most clear example showing that the interplay between recurrent mobility and epidemics goes beyond the redistribution of the population.

To shed more light on the role of the architecture of the mobility network, we now explore how the previous results are altered when varying the distribution of flows across the metapopulation. For this purpose, we fix $\delta=1$ and represent the same curves in Figure 10b, noticing that the rescaled epidemic threshold becomes independent of the permanence times. In contrast, as stated before, this dependence does appear if $\delta=0.4$, corresponding to a scenario in which residents in the leaf can either visit the hub or another leaf.

Note that the variability of the possible destinations visited by one individual is crucial to understand the impact of mobility on epidemic spreading. Although the interacting populations remain constant and independent of the permanence time for $p=1$, the recurrent nature of mobility allows each single individual to escape from the hub, where most contagions occur, and visit a leaf where they rarely get infected. This mechanism is promoted by higher return rates to the residence patch, which explains the consistent decrease of the epidemic threshold when increasing the permanence times τ.

Likewise, note that in the original MIR model, the rescaled epidemic threshold $\tilde{\lambda}_c$ does not depend on the recovery time of the pathogen μ^{-1}, as shown by Equation (38), so the expected outcome of mobility policies to fight an ongoing outbreak does not depend on the nature of the disease. Nonetheless, the introduction of the new time scale has proven the relevance of the

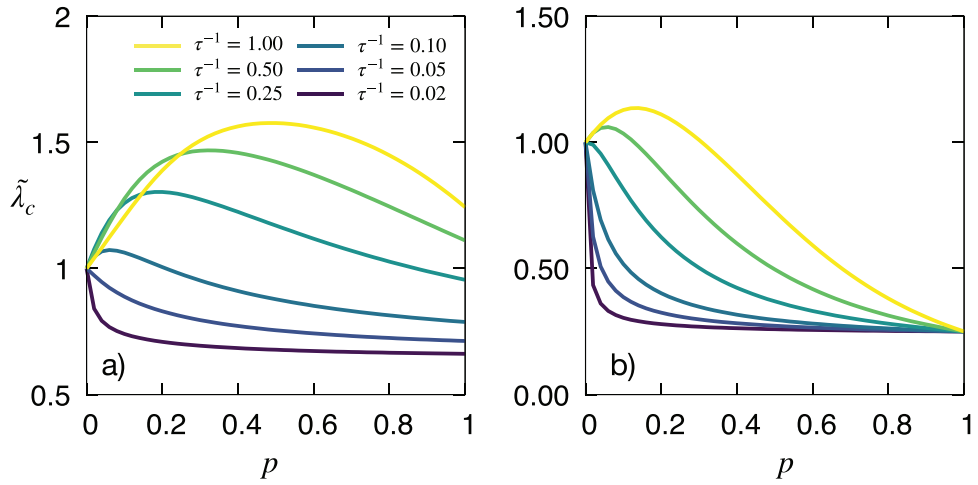

Figure 10. Rescaled epidemic threshold $\tilde{\lambda}_c$ as a function of the mobility parameter p and the return probability τ^{-1} (color code).The recovery rate is fixed to $\mu = 0.2$ and the underlying metapopulation is a star like configuration with $\kappa = 10$ leaves and $(\alpha, \delta) = (0.4, 0.4)$ (a) and $(\alpha, \delta) = (0.4, 1)$ (b). Reproduced with permission.[81] Copyright 2020, IOP.

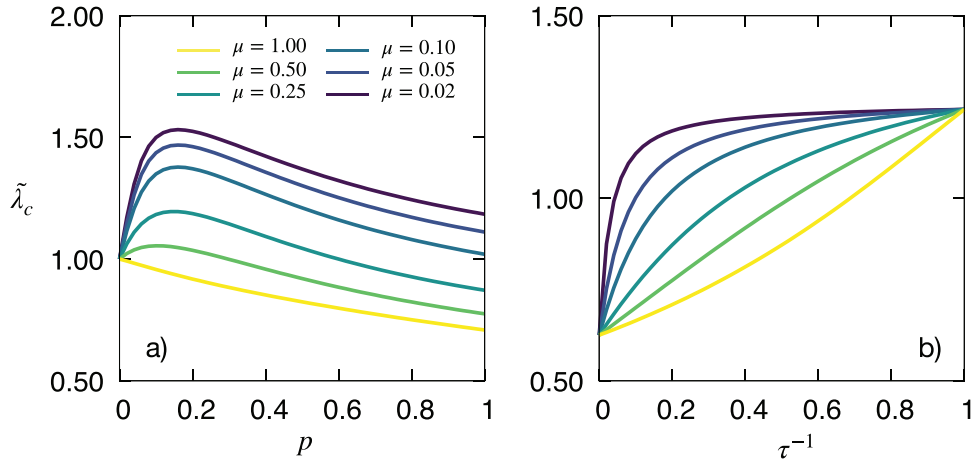

Figure 11. a) Rescaled epidemic threshold $\tilde{\lambda}_c$ as a function of the mobility parameter p and the recovery rate μ (color code). The return probability is fixed to $\tau^{-1} = 0.2$. b) Rescaled epidemic threshold $\tilde{\lambda}_c$ as a function of the return probability τ^{-1} and the recovery rate μ (color code). The mobility rate is fixed to $p = 1$. In both panels, the underlying metapopulation is a star like configuration with $\kappa = 10$ leaves and $(\alpha, \delta) = (0.4, 0.4)$. Reproduced with permission.[81] Copyright 2020, IOP.

alteration of the contact structures of the population and, more specifically, those corresponding to the interactions made by the infectious individuals.

To illustrate the interplay between the recurrent mobility and the time scale associated to epidemic processes, it is convenient to explore the behavior of the curves $\tilde{\lambda}_c(p)$ as a function the length of the infectious window, encoded in the recovery rate μ. Unlike in the original MIR model, **Figure 11** shows that varying the infectious period alters the impact of mobility on epidemic spreading. In particular, when $\mu^{-1} \ll \tau$, the infectious individual typically stays at one destination during the infectious period, which hinders the epidemic detriment and potentiate the negative effect provided by agents' accumulation inside the hub. In contrast, long infectious windows allow them to move and visit less vulnerable areas, which reduces the number of contagions and give rise to the epidemic detriment. Finally, Figure 11b represents the evolution of the rescaled epidemic threshold as a function of the permanence time for different infectious windows by fixing $p = 1$. The steeper slope of the epidemic threshold for small infectious periods confirms that, rather than the absolute value of the permanence time τ, its relative value compared with the typical infectious window is key to understand how the trip duration penalizes the epidemic detriment.

5.4. MIR Model with Heterogeneous Contact Patterns

The introduction of the permanence times in the MIR model reveals that the variation of the contact structures of the population plays a crucial role in the emergence of the epidemic detriment. However, note that, so far the MIR model and its explored variants assume the number of contacts of each agent to be an extensive variable depending on the population gathered in each geographical area. This way, the effect of changing the

set of individuals with whom an agent interacts is intermingled with the variation of the overall number of contacts. In general, this fact makes it difficult to attribute the main mechanism responsible for the epidemic detriment.

Furthermore, one of the most important limitations of the frameworks based on metapopulations is that they usually follow mean-field approaches consisting in considering all the individuals of a given subpopulation as statistically equivalent agents. A few examples can be found in the literature relaxing the latter assumption to accommodate different types of individuals within the same subpopulation. For instance, Apolloni et al.[85] define two different types of individuals and study how the coupling between the hosts' mobility and the contact matrix governing their contact shapes epidemic spreading. Bosetti et al.[86] address the impact of the degree of mixing between the Turkish population and the Syrian refugees on epidemic spreading. Likewise, multiple extensions of the MIR model have been proposed to model the influence of socioeconomic diversity on the spatial unfolding of outbreaks[62] or study the spread of SARS-CoV-2 across age-structured populations.[19]

Nonetheless, in all of them, it is assumed that individuals make the same number of interactions within each group, thus hindering the crucial role of heterogeneous contact distributions in epidemic spreading, as found in the models studied on contact networks.[8] The first attempt to overcome both limitations was proposed by Ruan et al. in ref. [87], where the authors study the diffusion of epidemics in a simple metapopulation composed of two coupled patches with inner structures. The model assumes that each patch displays its own contact network involving the total number of agents in the system. To couple the inner structure of each patch with human mobility, the model assumes that each individual has a residential patch and that the links of each network are activated according to whether each agent decides to stay in his/her associated patch or instead moves to the other one. Interestingly, in spite of the modeling differences with respect to the MIR model, the authors found the epidemic detriment in some regions of the parameters' space, thus highlighting the ubiquity of this counter-intuitive behavior induced by the existence of recurrent mobility patterns.

To generalize the analysis of the interplay between contact structures and mobility to more complex metapopulations, Cota et al.[88] propose a new extension of the MIR model in which each individual carries an attribute, the degree or number of contacts k, which is inherent to her/him and is not altered when visiting different locations from her/his residential node. Moreover, the authors abandon the usual mean-field assumption and instead consider a heterogeneous mean field scenario within each subpopulation so that the individuals from the same residential patch are divided into different degree classes, whose members are assumed to be equivalent.

In terms of the different processes of the original MIR model described in Section 4, the movement and returns stages remain intact whereas the new dynamical rules introduced in this work alter the Interaction stage. In particular, after the population is redistributed across the system as a consequence of their movements, each agent draws k connections which are randomly established with those agents sharing his/her location. In structural terms, apart from the number of patches N_p, the mobility matrix $\mathbf{R}$ and the sizes of each subpopulation $\{n_i\}$, the metapopulation is characterized by the degree distributions associated with each different patch $\{P_i(k)\}$. In what follows, the term degree refers to the number of contacts of each individual rather than to the number of connections of each subpopulation in the mobility network.

Specifically, to further characterize the epidemic detriment, the authors generalize the star-like metapopulation introduced in Section 5. Regarding the degree distributions, it is assumed that all the individuals from the leaves make $\langle k\rangle_l$ contacts, so that their degree distribution is given by

$$P_l(k) = \delta_{k\langle k\rangle_l} \tag{47}$$

In its turn, to introduce contact heterogeneities, the degrees of individuals from the hub follow a bimodal distribution, splitting the population into agents with a single contact and others with k_{max} interactions. In this sense, the share of population belonging to each group is governed by a new parameter denoted by η. Therefore

$$P_h(k) = \eta\delta_{k1} + (1-\eta)\delta_{kk_{max}} \tag{48}$$

Note that the nth moment of the hub's connectivity distribution is

$$\langle k^n\rangle_h = \sum_k k^n P_h(k) = \eta + (1-\eta)k_{max}^n \tag{49}$$

In particular, fixing the average degree as $\langle k\rangle_h$ automatically determines η, yielding

$$\eta = \frac{k_{max} - \langle k\rangle_h}{k_{max} - 1} \tag{50}$$

It is worth remarking that the latter configuration introduces two flavors of contact heterogeneities. First, the bimodal distribution of the contacts made by hub' residents induces local contact heterogeneities there. Likewise, the possible different average degree between individuals from the hub and the leaves represent some sort of global heterogeneity, quantifying how different individuals from distinct locations are. To control this global heterogeneity, it is useful to define $\langle k\rangle_l = \beta\langle k\rangle_h$ with $\beta \in (0, 1]$.

In the MIR model with heterogeneous contact patterns, the epidemic threshold reads as

$$\lambda_c = \frac{\mu}{\Lambda_{max}(\mathbf{M})} \tag{51}$$

where the elements of the new critical matrix $\mathbf{M}$ are given by

$$M_{ij} = \langle k^2\rangle_j \left[(1-p)^2\frac{\delta_{ij}}{Q_i} + p(1-p)\left(\frac{R_{ji}}{Q_i} + \frac{R_{ij}}{Q_j}\right) + p^2\sum_l \frac{R_{il}R_{jl}}{Q_l}\right] n_j \tag{52}$$

In the latter expression, $\langle k^2\rangle_j$ represents the second moment of the degree distribution of the patch j and Q_i the total number of edges inside patch j after all the movements have taken place. Accordingly

$$Q_i \equiv \sum_k k \sum_j \left[(1-p)\delta_{ij} + pR_{ji}\right] n_j P_j(k) \tag{53}$$

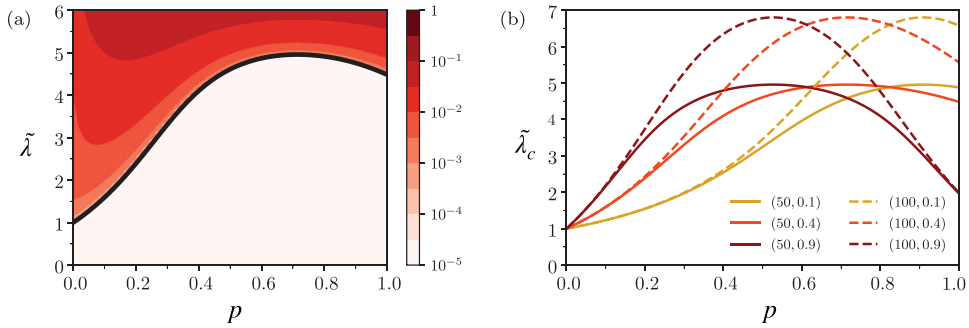

Figure 12. Dependence of the epidemic threshold on the mobility parameter p. The underlying metapopulation is the star-like configuration with $\kappa = 10$ leaves. All patches are uniformly populated ($\alpha = 1$) and the average connectivity of both hub and leaves is fixed to $\langle k\rangle_h = \langle k\rangle_l = 5$, so that $\beta = 1$. a) Comparison of the theoretical epidemic threshold obtained using Equation (51) (solid line), scaled by its value for $p = 0$, and the steady values of the epidemic size ρ (color code) for $(k_{max}, \delta) = (50, 0.4)$. b) Rescaled epidemic threshold $\tilde{\lambda}_c$ for different configurations (k_{max}, δ), shown in the legends, with solid and dashed lines for $k_{max} = 50$ and 100, respectively. Reproduced with permission.[88] Copyright 2021, IOP.

It is also worth remarking that matrix **M** qualitatively resembles the critical matrix obtained in the MIR model in Equation (20). Indeed, the four different contributions to the matrix elements encode the same microscopic processes but are differently weighed according to the modified interaction rules. This reveals the generality of the mobility scheme introduced in this review and how the MIR model model can be easily extended to cover more complex dynamics.

Figure 12a shows that the estimation for the epidemic threshold accurately captures the transition from the disease-free to the endemic state. Recall that in this framework, at variance with the models previously presented, agents preserve their number of interactions regardless of the place to which they move. This way, mobility does not shape the number of interactions of the population and therefore the epidemic detriment observed in the figure cannot be justified with macroscopic arguments based on the redistribution of the population.

From the elements of the critical matrix **M**, we immediately realize that, when $p = 0$, the epidemic threshold matches that arising from the HMF equations originally proposed for contact networks. The connection between this model and the HMF approach on contact networks reveals that the epidemic detriment could emerge as a result of dismantling the contact structures of individuals inside the hub, where localized endemic states persists in the static case, because of the recurrent mobility.

Decoupling the volume of interactions of each individual and its location allows discriminating the role of both contact heterogeneities and flows distribution in shaping the epidemic threshold. To do so, it is convenient to rely again on a star-like metapopulation in which global heterogeneities are neglected ($\beta = 1$) and the population is uniformly distributed, so that $\alpha = 1$. In this setup, either the local heterogeneities governed by k_{max} or the architecture of the mobility network governed by δ are varied.

Qualitatively, Figure 12b proves that the position of the peak p^* is determined by the mobility flows of the network but is independent on the local contact heterogeneities. Specifically, the peak is anticipated as δ increases, for the scarce overlapping between the mobility patterns of the individuals from the hub and the leaves reduces the beneficial effect of their mixing. In contrast, note that the exact value of the peak of the epidemic threshold $\lambda(p^*)$ is the same regardless of the position of the peak. Instead, it is increased as the parameter k_{max} increases, that is, as more vulnerable the hub is.

Finally, the authors illustrate the effect of the population asymmetry α on the peak of the epidemic threshold. Apart from the parameter β, it is convenient to define a new parameter γ to control global heterogeneities so that $\langle k^2\rangle_l = \gamma\langle k^2\rangle_h$. Note that the specific degree distributions of both hubs and leaves impose a constraint on these values, which must fulfil

$$\gamma = \frac{\beta^2\langle k\rangle_h^2}{\langle k\rangle_h\left(k_{max}+1\right) - k_{max}} \tag{54}$$

Figure 13 represents the value of the rescaled epidemic threshold at the peak as a function of the population asymmetry α and the parameters controlling the heterogeneities, β in (a) and γ in (b). The first striking result in both panels is that the epidemic peak is considerably reduced as the population is asymmetrically distributed, approaching $\tilde{\lambda}_c(p^*) = 1$ when $\alpha \to 0$. This behavior is observed because, as the leaves' population becomes negligible with respect to the hub's one, the agents from the leaves hardly alter the degree distribution of the residents in the hub.

Furthermore, note that, for a fixed β value, decreasing γ leads to an increase of the peak, thus highlighting a higher beneficial effect of the mobility. This effect is rooted in the fact that both subpopulations become more different among each other because of the higher k_{max} value needed to decrease γ. Likewise, the constraint posed by Equation (54) makes the epidemic threshold increase with β as a result of the higher k_{max} value to keep γ constant.

5.5. Epidemic Detriment as Delocalization Processes on Complex Networks

We have so far thoroughly described epidemic detriment due to spatial homogenization of populations caused by recurrent mobility.[61,88] This mechanism can be suited more generically as the delocalization process of the epidemic activity,[89] revised with some examples in this section. Localization phenomena driven by disordered inhomogeneities play a central role on condensed matter physics and can change drastically the

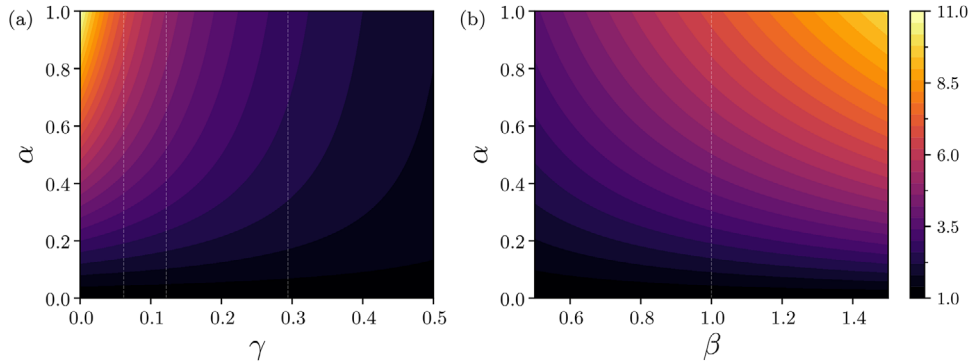

Figure 13. Peak of the rescaled epidemic threshold $\tilde{\lambda}_c(p^*)$ as a function of α, β, and γ, with $\langle k\rangle_h = 5$. a) all patches have the same average connectivity, with $\beta = 1$ while the local heterogeneity of the hub is modulated by γ. Dashed lines correspond to the values of γ for $k_{max} = 100$, 50, and 20, from left to right. b) The plot considers a fixed value of $\gamma \approx 0.0617$, corresponding to $k_{max} = 100$ when $\beta = 1$, tuning the connectivity of the leaves with β. The population asymmetry is modulated by α for all cases. Reproduced with permission.[88] Copyright 2021, IOP.

nature of the critical phenomena in both equilibrium[90,91] and nonequilibrium[91–93] systems. The ubiquitous heterogeneous structures of networks, where many dynamic processes take place, are source of many localization phenomena.[94–97] Consider the fundamental SIS epidemic model on unweighed and undirected networks with adjacency matrix **A**, in which each node represents a single individual which can be infected or susceptible. The continuous time dynamics involves the spontaneous healing rate μ and the infection rate per contact λ. The quenched mean-field (QMF) theory[98] for the probability ρ_i that a node i is infected is given by[99,100]

$$\partial_t \rho_i = -\mu\rho_i + \lambda(1-\rho_i)\sum_j A_{ij}\rho_j \tag{55}$$

which yields an epidemic threshold $\lambda_c = \mu/\Lambda_{max}(\mathbf{A})$.[99,100] The same dependence with the inverse of the adjacency matrix is obtained for discrete-time SIS dynamics.[67,101] This result combined with the fact that the largest eigenvalue of **A** diverges with the network size N for networks with power–law degree distributions $P(k) \approx k^{-\gamma}$[102] results in the remarkable consequence that the QMF epidemic threshold goes to zero in the thermodynamic limit $N \to \infty$ for any value of the degree exponent γ.[98]

The QMF result, however, has the drawback that ρ_i is proportional to the leading eigenvector corresponding to the largest eigenvalue[99,100] of **A** which, in the case of random networks with power–law degree distribution, is localized in a finite set of nodes for $\gamma > 5/2$[99,103] implying that the QMF epidemic prevalence could not correspond to the onset of an endemic phase.[104] However, the existence of an endemic phase for the SIS on random power-law networks with $\gamma > 3$ for any value of $\lambda > 0$ was rigorously proved by Chatterjee and Durret[105] in complement to the previous consensus with respect to the asymptotically null epidemic threshold for scale-free networks with $\gamma < 3$[106,107], irrespective of correlation patterns.[108,109] Furthermore, Boguña et al.[110] put the rigorous proof of ref. [105] into sound physical grounds in terms of a feedback mechanism in which the hubs and their k neighbors are able to sustain a local epidemic activity for a lifespan $\tau \approx \exp(a\lambda^2 k/\mu^2)$, where a is a $\mathcal{O}(1)$ constant, which is much longer than the typical time, increasing algebraically with k, for a rare fluctuation generated in a locally active hub to ignite the epidemic in other distant hubs. This mutual long-range activation of hubs produces an actual endemic phase for any nonzero infection rate and any finite value of γ. The ideas of ref. [110] were generalized into a criterion to determine whether the activation of an epidemic process is driven by a localized activity of hubs or not.[78,111] The criterion is to compare the lifespan of epidemic activity in star subgraphs centered on the network's hubs with the characteristic time for mutual activation of hubs. If the former exceeds the latter, the endemic phase is driven by localized activity of hubs. Otherwise, the transition happens collectively involving extensive parts of the networks.

Epidemic detriment can emerge as a delocalization process on networked structures as some model parameters are tuned, as does recurrent mobility rate in the MIR model. A first example is the inclusion of waning immunity in the SIS model configuring a susceptible-infected-recovered-susceptible (SIRS) dynamics, where an infected individual becomes recovered and immune to infections with rate μ but returns to the susceptible compartment after an average immunity time $1/\alpha$.[112] While, on the one hand, it is intuitively expected that increasing the immunity time promotes epidemic detriment, on the other hand, the mean-field theory yields exactly the same threshold of the SIS model $\lambda_c = \mu/\Lambda_{max}(\mathbf{A})$ for the SIRS dynamics, independently of the waning immunity rate α.[78] However, extensive stochastic simulations[78] corroborate not only the epidemic detriment as immunity time increases, but a drastic change happens for degree exponents $\gamma > 3$: the SIRS epidemic threshold converges to a nonzero value in the thermodynamic limit for any finite waning immunity rate in sharp contrast with SIS. **Figure 14**a shows the epidemic detriment as a function of the immunity time $1/\alpha$ for SIRS on large networks with power law-degree distributions with different values of γ generated according to the uncorrelated configuration model.[113] The delocalization is due to the fact that the lifespan for epidemic activity in an isolated hub of degree k increases algebraically as $\tau \approx k^{\alpha/\mu}$,[78] while the time required for mutual infection of hubs scales as $\tau^{inf} \approx N^{\gamma(\lambda)}$ where $\gamma \to \infty$ as $\lambda \to 0$. Therefore, for sufficiently low value of λ, the mutual infection time exceeds the lifespan of the largest hub and the epidemic processes cannot be sustained by activity localized in hubs. For scale-free networks with $\gamma < 3$, hubs are close enough to grant almost direct mutual reinfection and the threshold remains vanishing as $N \to$

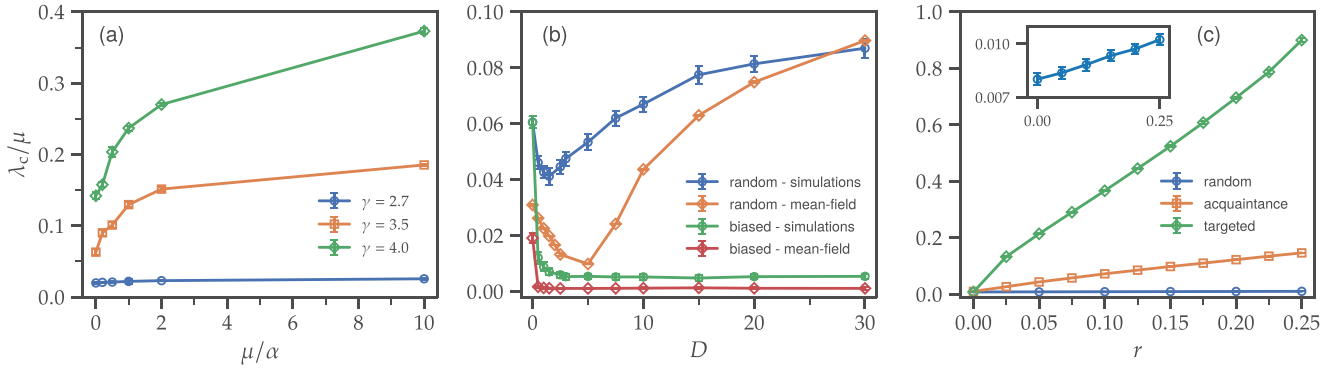

Figure 14. Epidemic detriment for networks with power-degree distribution due to a) waning immunity in SIRS, b) diffusion, and c) immunization in SIS models. Random networks with $N = 10^7$ nodes used in (a,b) and $N = 10^6$ nodes used in (c) were generated according to the uncorrelated configuration model.[113] The degree exponent is fixed to $\gamma = 3.5$ for (b) diffusive SIS and $\gamma = 2.3$ for (c) immunization strategies; see refs. [78, 114, 115] for details. The inset in (c) shows the curve for random immunization in a narrower scale.

∞. In summary, temporary immunity weakens the feedback mechanism of reinfection of hubs by its neighbors, which were infected by the hub itself and, consequently, epidemic activity localization is strongly damped implying in epidemic detriment.

A second example of epidemic detriment involves the SIS model with diffusion on networks, where the state of two nearest neighbors i and j are exchanged with rate D_{ij}. Since random walk dynamics on networks leads to the accumulation of particles on hubs,[46] where infected individuals are more contagious, one intuitively expects that diffusion would facilitate epidemic spreading. Silva and Ferreira[114] investigated two rules corresponding to a diffusion rate per node equal to D in both cases. In the random diffusion model, in which a node i is randomly selected to perform a movement, the destination j is chosen with equal chance among the nearest neighbors of i, such that the diffusion rate is $D_{ij} = DA_{ij}/k_i$, where k_i is the degree of node i. In a degree-biased diffusion set up,[116–118] the movement departing from node i is preferentially directed toward high degree nodes with rate $D_{ij} \propto DA_{ij}k_j/k_i$. The QMF equation for SIS with diffusion is given by[114]

$$\partial_t \rho_i = -\mu\rho_i + \lambda(1-\rho_i)\sum_j A_{ij}\rho_j - \rho_i \sum_j D_{ij}(1-\rho_j) + (1-\rho_i)\sum_j D_{ji}\rho_j \tag{56}$$

The meaning of each term is straightforward. A linear stability analysis around $\rho_i = 0$ provides the Jacobian matrix $J_{ij} = -(\mu + D)\delta_{ij} + \lambda A_{ij} + D_{ji}$ and the threshold determined by the condition $\Lambda_{\max}(\mathbf{J}) = 0$. Epidemic thresholds of diffusive SIS model on power–law networks are presented in Figure 14b for both stochastic simulations and numerical solution of the QMF theory. Low rates of random diffusion is beneficial for epidemic spreading, but diffusion becomes detrimental for high rates. In the case of biased diffusion, mobility always facilitates epidemic spreading. Some analytical insights are obtained from a mean-field theory on a leaking star graph defined as follows. A center (the hub) is connected to K leaves (the neighbors) of degree $\langle k\rangle$ (the outer world). The outer $\langle k\rangle - 1$ neighbors of the leaves are assumed to be permanently susceptible implying that an infected individual can leak outward the star graph but the converse cannot happen. For the limit case $K \gg \langle k\rangle$, that mimics a hub immersed in a network of average degree $\langle k\rangle$, the epidemic thresholds for biased and random diffusion models become

$$\lambda_c \simeq \mu\frac{2D+\mu}{DK} \tag{57}$$

and

$$\lambda_c \simeq \frac{\langle k\rangle(\mu+D)^2 - D^2}{DK} \tag{58}$$

respectively. While the biased diffusion model presents a monotonically decreasing epidemic threshold, the random diffusion model presents epidemic detriment for $D/\mu > \sqrt{\langle k\rangle/(\langle k\rangle - 1)}$.

The relation between delocalization and epidemic detriment or enhancement can be settled as follows. In biased diffusion hubs always attracts infected individuals since even when an infected individual moves out the hub its tendency is to move back to it in the next step. While, on the one hand, random diffusion also favors movement toward higher degree nodes, on the other hand, if D is too high the infected individual leaves a hub very shortly, reducing its number of contacts and consequently its spreading capacity. So, the epidemic detriment in diffusive SIS on networks comes from the competition between migration toward hubs and the amount of time that infected individuals remains there, both boosted by the diffusion rate D.

As a last example of epidemic detriment that can also be associated with delocalization of epidemic activity, we discuss strategies of immunizing a fraction r of the nodes of the network.[119–121] An extensive revision of vaccination models can be found elsewhere.[121] Here, we discuss the breakdown of epidemic localization due to immunization using a HMF approximation where the state of nodes depend only on their degree k.[106] Without immunization the epidemic threshold is given by $\lambda_c = \mu\langle k\rangle/\langle k^2\rangle$.[106] The case of random immunization leads to a correction in the epidemic threshold given by[119]

$$\lambda_c = \frac{\mu}{1-r}\frac{\langle k\rangle}{\langle k^2\rangle} \tag{59}$$

For the case of scale-free networks with $\gamma < 3$, $\langle k^2 \rangle$ diverges in the thermodynamic limit and the epidemic detriment is not sufficient to restore a nonzero threshold.

A similar analysis can be constructed for the QMF theory for the non immunized nodes as follows

$$\partial_t \rho_i = -\mu \rho_i + \lambda(1-\rho_i) \sum_{j=1}^{N} A_{ij}(1-r_j)\rho_j \tag{60}$$

where $r_j = 1$ if the node j was immunized and $r_j = 0$ otherwise. The problem is equivalent to a SIS dynamics on a modified adjacency matrix $A^*_{ij} = A_{ij}(1-r_j)$ with epidemic threshold $\lambda_c = \mu/\Lambda_{\max}(\mathbf{A}^*)$. Since the immunization is done at random, the average over an ensemble of immunization realizations leads to the epidemic threshold

$$\lambda_c = \frac{\mu}{(1-r)\Lambda_{\max}(\mathbf{A})} \tag{61}$$

implying that the epidemic detriment is not capable of restoring a finite epidemic threshold for any value of the degree exponent γ.

In a targeted immunization the nodes are immunized in decreasing degree order, implying that hubs are immunized preferentially. Consequently, all nodes of degree above k_*, given by $r = \sum_{k=k_*}^{\infty} P(k)$, will be immunized. Using $P(k) \simeq (\gamma-1)k_{\min}^{\gamma-1}k^{-\gamma}$ in a continuous approach to replace the summation by an integral, we obtain $k_* = k_{\min} r^{-1/(\gamma-1)}$, where $k_{\min}$ is the minimum degree of the network. So, for any value of $r > 0$ the degree distribution has a finite upper cutoff in the thermodynamic limit and nonzero threshold will occur since localization due to self-activation of hubs is not at work for small λ. A clever strategy is the acquaintance immunization[120] where a contact of a randomly selected node is immunized. Its inspiration is the fact that the degree distribution of contacts is given by $P_{\rm nn}(k) = kP(k)/\langle k \rangle$[122] such that the hubs can be chased using contact tracing of randomly chosen nodes. Therefore, the probability that a node of degree larger than k is chosen to be immunized is

$$\Pi(k) \simeq \int_k^{\infty} P_{\rm nn}(k)\mathrm{d}k = \left(\frac{k_{\min}}{k}\right)^{\gamma-2} \tag{62}$$

An upper cutoff for the node degree can be estimated when the expected number of immunized nodes of degree larger than k_* is equal to the total number of these nodes

$$rN\Pi(k_*) = N\int_{k_*}^{\infty} P(k)\mathrm{d}k = N\left(\frac{k_{\min}}{k_*}\right)^{\gamma-1} \tag{63}$$

which translate into $k_* = k_{\min} r^{-1}$, which is again finite for a nonzero fraction of immunized nodes implying once again in a finite threshold. The epidemic detriment is shown in Figure 14c for the three aforementioned immunization strategies.

The epidemic detriment is present in the whole interval of r, below the percolation threshold, determining the fraction of removed nodes above which the network is fragmented into small components,[120,122] meaning that the largest connected component has a size of order N. As expected, the targeted immunization has the strongest effect, followed by acquaintance and random immunization strategies, the last one being almost negligible. It is important to remark that not only the hubs but also the average distance among nonimmunized nodes are altered by immunization and both features impact the level of epidemic detriment.[115]

Even in the case of random immunization, which does not alter the largest degree, the average distances increases a little justifying the mild epidemic detriment observed in the inset of Figure 14c. Costa and Ferreira[115] analyzed epidemic detriment in a scenario of nonmassive immunization where a fraction of immunized nodes is far below the percolation threshold. It was claimed that the interplay between both structural aspects, the average degree of the most connected hubs and average shortest distance among them, are fundamental for determining the epidemic detriment, which can be very effective even for a nonmassive and weakly supervised immunization by altering the nature of the epidemic transition from a specific motif (hubs or other subextensive structures) to a collectively driven activation.

6. Cities' Vulnerability and Mobility

Finally, we illustrate how all the knowledge acquired when applying the MIR model to synthetic networks has been leveraged to characterize how daily human mobility affects cities' vulnerability to epidemic outbreaks. Following the spirit of different works within the so-called science of cities,[123–126] Hazarie et al.[75] explore hierarchies and regularities in cities' structures to explain those factors shaping their vulnerability to epidemic outbreaks. For this purpose, they rely on the LouBar method proposed in ref. [70], which allows a dimensionality reduction of the mobility networks. This way, the LouBar method enables to encapsulate superficial cultural, structural or historical differences existing between different cities and focus on the mesoscopic structures governing the flows and agents' distribution across them. In some sense, this method resembles the renormalization group widely studied in statistical physics,[127] which is able to classify dynamics of different nature within the same universality class.

6.1. LouBar Method

The LouBar method establishes a hierarchical structure within the different geographical areas inside a city as a function of a given attribute of interest. This attribute may be related to demographic features such as the population and the population density or to socioeconomic indicators such as the GDP per capita. In practical terms, the LouBar method is a non-parametric method which allows classifying the patches in a metapopulation in different levels according to their contribution to the Lorenz curve of the attribute of interest.

If the variable of interest x is continuous and governed by a given probability function $f(x)$ and cumulative distribution $F(x)$, the Lorenz curve $L(F(x))$ is defined as

$$L(F(x)) = \frac{1}{\langle x \rangle}\int_{x_{\min}}^{x} x' f(x')\mathrm{d}x' \tag{64}$$

where the factor $\langle x \rangle$ is included to ensure that $L(1) = 1$. In economic terms, the value $L(x)$ represents the proportion of the total

wealth of a system shared between those whose income is lower than x. Given this definition, the Lorenz curve has been used to quantify economic inequalities via the Gini coefficient. This coefficient is defined as the area between the Lorenz curve and the curve corresponding to an egalitarian economic distribution provided by $L(F(x)) = F(x)$.

Note that, in a metapopulation, the variables are discrete and correspond to different attributes of the patches. Assuming that the values are sorted so that $x_1 < \ldots < x_{N_p}$, the Lorenz curve is computed as

$$L\big(F(i)\big) = \frac{\sum_{j=1}^{i} x_j}{\sum_{j=1}^{N_p} x_j} \tag{65}$$

with

$$F(i) = \frac{i}{N_p} \tag{66}$$

Once the Lorenz curve $L(F)$ is constructed parametrically, the LouBar method draws the tangent line to the curve at (1,1) and finds the intersection point of the latter with the x-axis, setting a threshold denoted by F^*. From Equation (65), the intersection point is computed as

$$F^* = 1 - \frac{\langle x \rangle}{x_n} \tag{67}$$

The intersection point F^* allows discriminating those areas contributing to the inequalities of the distribution. In particular, for egalitarian distributions, that is, $x_n = \langle x \rangle$, the intersection point is $F^* = 0$ and, consequently, all the patches are equivalent. As the value x_n grows with respect to the average, the intersection point F^* adopts intermediate values separating the patches into two subsets. In this sense, a patch i is identified as a hotspot when $F(i) > F^*$.

In a nutshell, the LouBar method allows coarse-graining the patches in a metapopulation as a function of their similarities according to a given property. One application of this method was proposed by Bassolas et al. in ref. [74] where the attribute of interest is the number of flows departing from each area. Applying the method iteratively, the authors embed the complex nature of the mobility network into a hierarchical structure formed by the different hotspot levels and their aggregated connections. Interestingly, they derive an indicator, the hierarchical flow, quantifying to what extent the flows connect hotspots within the same level in different cities, and find that there exists a correlation between the latter indicator and different environmental and social features such as the level of pollution or the share of public transport.

6.2. MIR Model with Hotspots

Regarding epidemic spreading, the LouBar method can be applied to shed some light on the interplay between mobility and the epidemic threshold in real cities. Given its relevance for the spread of airborne diseases, the authors in ref. [75] assume that the function f governing the number of contacts inside each patch is a monotonically increasing function with the population density. In particular, for the sake of simplicity, they choose $f(i) = \tilde{n}_i/a_i$, being $\tilde{n}_i$ the effective population gathered inside patch i and a_i its area. The results described in the previous sections suggest that the detrimental effect of mobility should be hindered in those cities where the flows are concentrated around the most densely populated areas. In this scenario, mobility does not allow the population to escape from the most vulnerable areas, therefore reducing the beneficial effect of contacts' variability. To quantify this concentration, the authors extract the population density hotspots and define a new indicator κ, whose value for each city k is given by

$$\kappa_k = \frac{\sum_{i,j \in H_k} T_{ij}^k}{\sum_{i,j} T_{ij}^k} \tag{68}$$

where $H(k)$ encodes the set of hotspots within city k and that T_{ij}^k denotes the flows going from patch i to patch j inside city k. Note that this metric lies in the range $0 \leq \kappa \leq 1$. An illustrative scheme of the dimensionality reduction here proposed is represented in **Figure 15**a. To have a fair comparison of the effect of the mobility in two cities with disparate population densities, the authors consider the rescaled epidemic threshold $\tilde{\lambda}_c$ at $p = 1$, which in this model is given by:

$$\tilde{\lambda}_c = \frac{\lambda_c(p=1)}{\lambda_c(p=0)} = \frac{d_{\max}}{\Lambda_{\max}(\mathbf{M}_{p=1})} \tag{69}$$

where $d_{\max}$ represent the largest population density observed within the patches of each city.

Figure 15b represents the rescaled epidemic threshold as a function of the κ value of each city in each of the four countries analyzed in this study. In all the cases, a moderate negative correlation between both variables is found. As a proof of concept, the authors fit the curve of each country to a power-law decay $\tilde{\lambda}_c \approx A\kappa^{\beta}$ by using least-squares regression, obtaining negative values in all the cases for the exponent β. The different values observed in these exponents may arise as a consequence of the different spatial resolutions with which the mobility networks in each country are constructed or obey further structural features omitted by the LouBar method.

6.3. Interventions on the Mobility Matrix

To confirm the negative effect of the concentration of mobility flows around hotspots for cities' vulnerability, the authors perform an intervention on the mobility network consisting in removing all the flows connecting different hotspots and distributing them among the neighboring suburbs, that is, those areas not labeled as hotspots, preserving the proportions as dictated by the original matrix $\mathbf{R}$. In the following, this intervention is referred to as reshuffling intervention. The effect of such intervention is captured in **Figure 16**a, which presents a

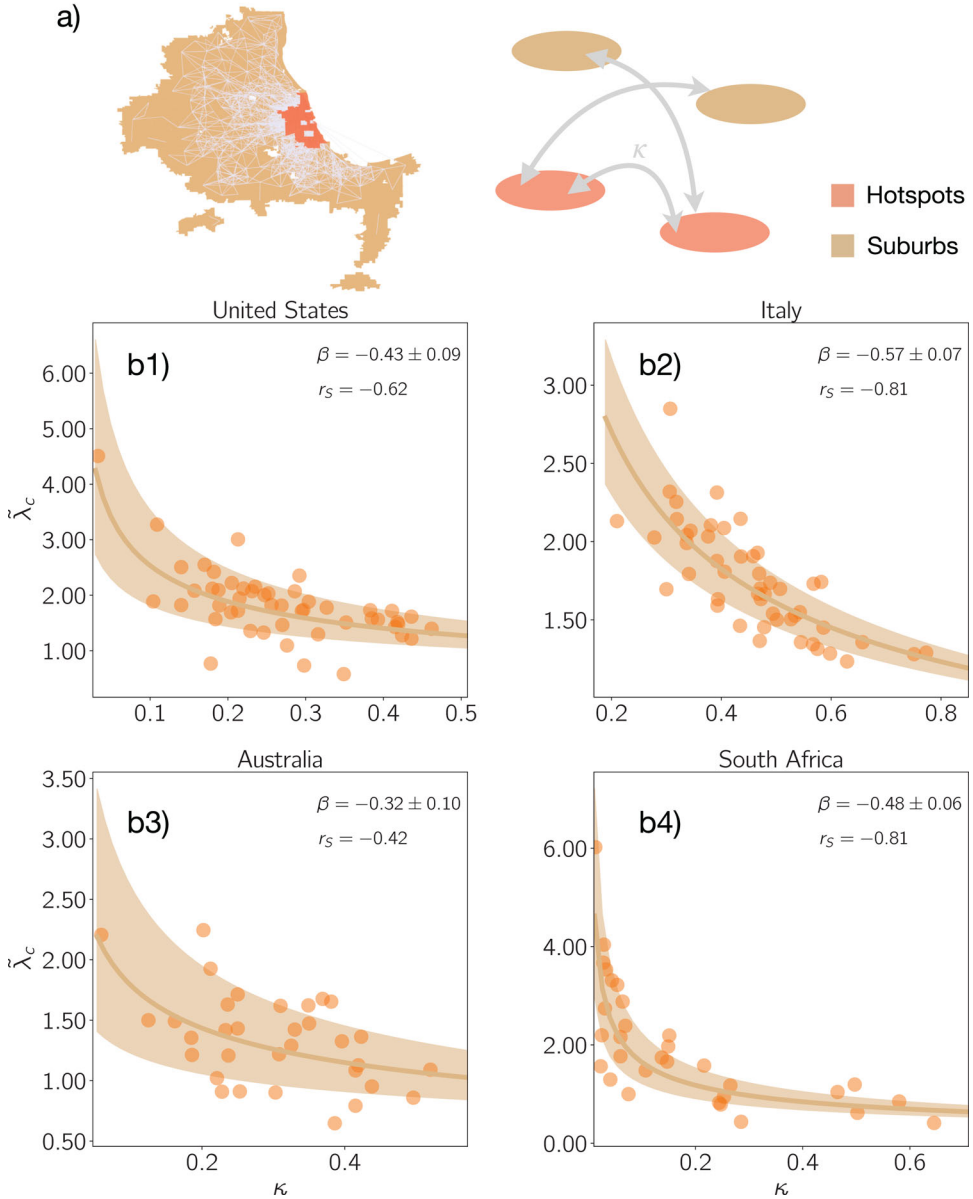

Figure 15. a) Mobility network of Chicago in the United States and its associated low-dimensional representation. The brown areas correspond to suburbs whereas the red areas identify the hotspots defined according to the population density. b1–b4) Rescaled epidemic threshold $\tilde{\lambda}_c$ as a function of the hotspot flow concentration κ for each of the cities analyzed in United States (b1), Italy (b2), Australia (b3), and South Africa (b4). In all these panels, the metric β is the exponent of the power-law function to which data are fitted in each country (see text for details) and r_S is the Spearman rank correlation coefficient relating the rescaled epidemic threshold values to the hotspots flow concentration. The shadowed region shows 95% confidence interval for the fitted dependencies. Reproduced with permission.[75] Copyright 2021, Springer.

histogram of the values for the ratio between the normalized threshold after and before the intervention, $\tilde{\lambda}_c^{\mathrm{MOD}}$ and $\tilde{\lambda}_c$ respectively. Note that most cities fall into the beneficial domain for which removing the flow between hotspots increases city' resilience. In contrast, there are a few cities, around 9% of the cities studied, for which the intervention is detrimental and accelerates epidemic spreading. The latter behavior is rooted in those details of the underlying density distribution which are overlooked when coarse-graining the flow between hotspots in κ. A breakdown of the cities classified according to the effect of the reshuffling intervention and their country is made in Figure 16b.

Despite the clear beneficial effect of removing the flows between hotspots, this intervention is not doable as a short-term reaction to an ongoing outbreak due to the long times needed to achieve the desired redistribution of the population across the neighboring suburbs. Instead, a more realistic intervention would be that of targeting specific individuals and forcing them to stay in their associated patches. It is worth stressing that this intervention does not entail the lockdown of this population at

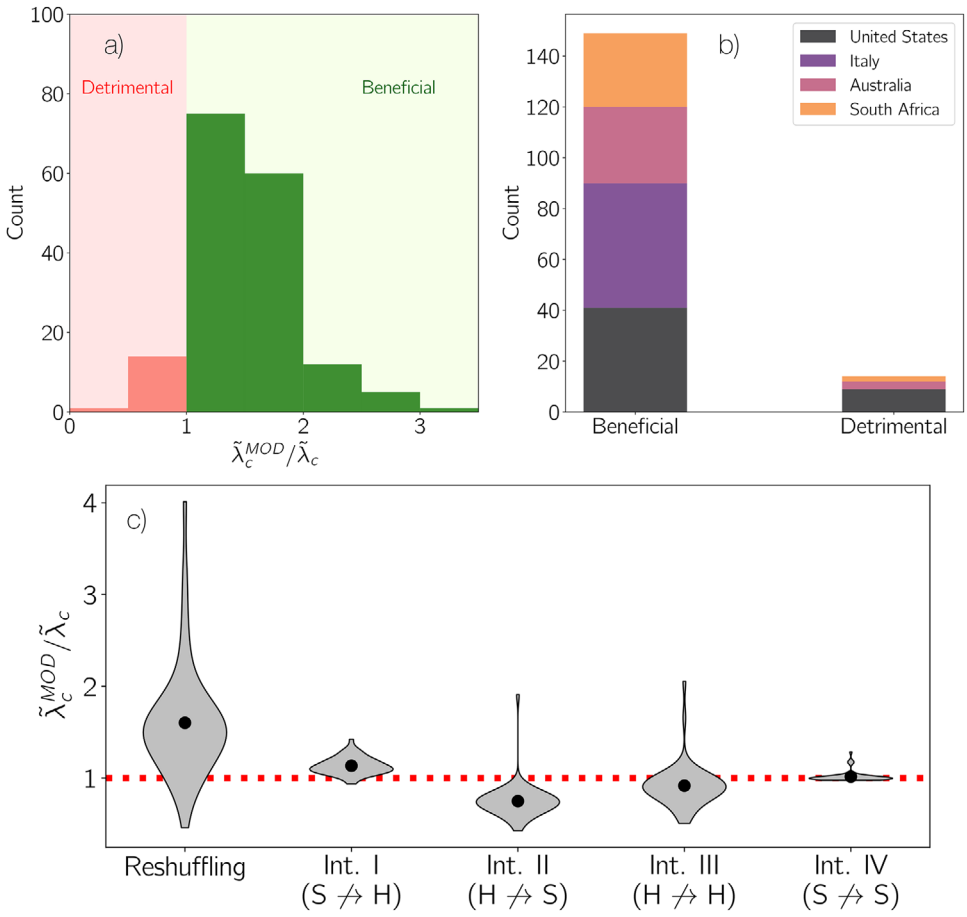

Figure 16. a) Histogram for the ratio between the rescaled epidemic threshold after the reshuffling intervention $\tilde{\lambda}_c^{MOD}$ and the original threshold $\tilde{\lambda}_c$, highlight two different types of cities: those for which this intervention is beneficial and those for which is detrimental. b) Breakdown of the cities belonging to each country (color code) as a function of the outcome of the reshuffling intervention. c) Distribution of the ratios following different intervention schemes for the US cities. The black dots represent the average of each distribution. For the sake of clarity, we explicitly indicate the flows affected in each intervention. For example, S ↛ H removes the flows from suburbs to hotspots and turns them into self-loops. The red dashed line highlights the case in which the interventions do not have any effect on the threshold. Reproduced with permission.[75] Copyright 2021, Springer.

home but only prevents the circulation of the targeted individuals across the metapopulation. The authors explore four different scenarios in which the flows connecting two categories of patches are deleted and converted into self-loops. The affected subpopulations are:

- Intervention I: Individuals moving from suburbs to hotspots.
- Intervention II: Individuals moving from hotspots to suburbs.
- Intervention III: Individuals moving from hotspots to hotspots.
- Intervention IV: Individuals moving from suburbs to suburbs.

Figure 16c summarizes the effects of deploying each of the interventions described in this section for the United States (US) cities. The first striking result in this figure is the asymmetric outcome of closing the flows involving individuals that move between hotspots and suburbs. Specifically, preventing residents in the suburbs from visiting the hub increases the city's resilience whereas removing the routes from hotspots to suburbs makes the city more vulnerable. To understand this asymmetry, we must recall that hotspots behave as contagion centers; hence, every intervention aimed at reducing the time spent by the population in these areas will be beneficial to stop the propagation of the disease. For this reason, intervention I works whereas in intervention II the spatial isolation of the outbreak is made at the expense of a higher exposure of the residents in the hub to the contagion sources, making it fail. Finally, acting on the flows connecting patches from the same category (namely interventions III and IV) does not alter the threshold on average because of the internal similarities within each category.

7. Conclusions

The great development of the international mobility network over the last 50 years has dramatically changed the course of pandemics. The removal of the physical gaps separating distant regions driven by this phenomenon has led to an inversion of the time scales responsible for global diffusion of outbreaks, making the spatial confinement of localized outbreaks practically unfeasible. In this scenario, capturing the factors shaping the

vulnerability of real cities upon the arrival of imported cases becomes indispensable to improve our preparedness to future pandemics.

In this review, we have revisited the different theoretical models proposed in the literature to explore the interplay between our daily recurrent movements and the spread of infectious diseases. The analysis of the different models reveals that the impact of recurrent mobility on epidemic spreading in real cities is not universal but is strongly influenced by their structural and demographic features and how human flows are distributed across them. This impact is the result of the trade-off between two antagonistic effects: on the one hand, mobility helps mixing the different subpopulations inside a city, thus resulting in a higher exposure of the overall population. On the other hand, mobility dismantles the contact structures responsible for the emergence of local outbreaks in the most vulnerable areas by allowing their population to be away from the focus on contagion.

The outcome of such competition depends on the infectiousness of the pathogen. While for highly infectious pathogens, the first mechanism prevails and mobility tends to accelerate the spread of diseases, in less dangerous scenarios the beneficial effect of the mobility becomes more relevant, giving rise to the epidemic detriment here analyzed. As a consequence, policies acting on the mobility of the population should be tailored for each specific disease and epidemic scenario.

The microscopic roots of the epidemic detriment shed light into its connection with other phenomena found when addressing epidemic spreading on contact networks, such as the vulnerability of heterogeneous configurations to targeted control policies or the increase of the epidemic threshold observed in temporal networks as a result of the time-varying nature of the interactions.[128] Likewise, the detriment of a process driven by hosts' movements is not a phenomenon restricted to the interplay between epidemics and mobility. For instance, it has been also been reported in genetics,[129–131] where the fixation of mutations in the population is hampered when high migration rates of the population are introduced.

From a practical point of view, characterizing correctly how the local transmission of a disease is affected by our daily urban rhythms becomes essential for the design of optimal interventions to increase cities' resilience to future threatening epidemic outbreaks. For this purpose, the theories developed thus far focusing on synthetic simple networks must move toward data-driven approaches incorporating the complex mobility patterns observed in real systems,[36] the multiscale nature of human mobility[33] or other socioeconomic layers shaping the spread of diseases such as the specific age-stratified contact matrices[132,133] or the existence of diverse social classes within the same population.[134]

Acknowledgements

D.S.P. and J.G.G. acknowledge financial support from the Departamento de Industria e Innovación del Gobierno de Aragón y Fondo Social Europeo (FENOL group E36-20R), from grant PID2020-113582GB-I00 funded by MCIN/AEI/10.13039/501100011033, and from Fundación Ibercaja and Universidad de Zaragoza (grant 224220). A.A. acknowledges financial support from Spanish MINECO (Grant No. PGC2018-094754-B-C21), Generalitat de Catalunya (Grant No. 2017SGR-896 and 2020PANDE00098), Universitat Rovira i Virgili (Grant No. 2019PFR-URV-B2-41), Generalitat de Catalunya (PDAD14/20/00001), ICREA Academia, and the James S. McDonnell Foundation (Grant No. 220020325). W.C. and S.C.F. acknowledges the final support of Coordenação de Aperfeiçoamento de Pessoal de Nível Superior—CAPES (Grant no. 88887.507046/2020-00), Conselho Nacional de Desenvolvimento Científico e Tecnológico—CNPq (Grants no. 430768/2018-4 and 311183/2019-0), and Fundação de Amparoá Pesquisa do Estado de Minas Gerais—FAPEMIG (Grant no. APQ-02393-18). The authors thank D. H. Silva for data of Figure 14b.

Conflict of Interest

The authors declare no conflict of interest.

Keywords

epidemics, human mobility, networks

Received: October 15, 2021
Revised: January 7, 2022
Published online:

[1] O. J. Benedictow, *The Black Death 1346-1353: The Complete History*, Boydell & Brewer, Woodbridge**2006**.
[2] *The World of Air Transport in 2018*, **2018**, https://www.icao.int/annual-report-2018/Pages/the-world-of-air-transport-in-2018.aspx (accessed: January 2021).
[3] D. Brockmann, D. Helbing, *Science* **2013**, *342*, 1337.
[4] V. Colizza, A. Barrat, M. Barthélemy, A. Vespignani, *BMC Med.* **2007**, *5*, 34.
[5] M. Tizzoni, P. Bajardi, C. Poletto, J. Ramasco, D. Balcan, B. Gonçalves, N. Perra, V. Colizza, A. Vespignani, *BMC Med.* **2012**, *10*, 165.
[6] M. U. G. Kraemer, C.-H. Yang, B. Gutierrez, C.-H. Wu, B. Klein, D. M. Pigott, O. C.-. D. W. Group†, L. du Plessis, N. R. Faria, R. Li, W. P. Hanage, J. S. Brownstein, M. Layan, A. Vespignani, H. Tian, C. Dye, O. G. Pybus, S. V. Scarpino, *Science* **2020**, *368*, 493.
[7] M. Gilbert, G. Pullano, F. Pinotti, E. Valdano, C. Poletto, P.-Y. Boalle, E. D. Ortenzio, Y. Yazdanpanah, S. P. Eholie, M. Altmann, B. Gutierrez, M. U. G. Kraemer, V. Colizza, *Lancet* **2020**, *395*, 871.
[8] R. Pastor-Satorras, C. Castellano, P. Van Mieghem, A. Vespignani, *Rev. Mod. Phys.* **2015**, *87*, 925.
[9] V. Belik, T. Geisel, D. Brockmann, *Phys. Rev. X* **2011**, *1*, 011001.
[10] D. Balcan, V. Colizza, B. Goncalves, H. Hu, J. J. Ramasco, A. Vespignani, *Proc. Natl. Acad. Sci. USA* **2009**, *106*, 21484.
[11] C. Panigutti, M. Tizzoni, P. Bajardi, Z. Smoreda, V. Colizza, *R. Soc. Open Sci.* **2017**, *4*, 160950.
[12] R. Moss, E. Naghizade, M. Tomko, N. Geard, *BMC Public Health* **2019**, *19*, 656.
[13] Z. Ruan, C. Wang, P. M. Hui, Z. Liu, *Sci. Rep.* **2015**, *5*, 11401.
[14] M. Mazzoli, A. Molas, A. Bassolas, M. Lenormand, P. Colet, J. Ramasco, *Nat. Commun.* **2019**, *10*, 3895.
[15] M. Tizzoni, P. Bajardi, A. Decuyper, G. Kon Kam King, C. M. Schneider, V. Blondel, Z. Smoreda, M. C. González, V. Colizza, *PLOS Comput. Biol.* **2014**, *10*, e1003716.
[16] H. Barbosa, F. B. de Lima-Neto, A. Evsukoff, R. Menezes, *EPJ Data Sci.* **2015**, *4*, 21.
[17] D. Soriano-Paños, J. H. Arias-Castro, A. Reyna-Lara, H. J. Martínez, S. Meloni, J. Gómez-Gardeñes, *Phys. Rev. Res.* **2020**, *2*, 013312.
[18] A. Wesolowski, N. Eagle, A. J. Tatem, D. L. Smith, A. M. Noor, R. W. Snow, C. O. Buckee, *Science* **2012**, *338*, 267.
[19] A. Arenas, W. Cota, J. Gómez-Gardeñes, S. Gómez, C. Granell, J. T. Matamalas, D. Soriano-Paños, B. Steinegger, *Phys. Rev. X* **2020**, *10*, 041055.

[20] G. S. Costa, W. Cota, S. C. Ferreira, *Phys. Rev. Res.* **2020**, *2*, 043306.
[21] H. S. Badr, H. Du, M. Marshall, E. Dong, M. M. Squire, L. M. Gardner, *Lancet Infect. Dis.* **2020**, *20*, 1247.
[22] E. Bertuzzo, L. Mari, D. Pasetto, S. Miccoli, R. Casagrandi, M. Gatto, A. Rinaldo, *Nat. Commun.* **2020**, *11*, 4264.
[23] R. Levins, *Bull. Entomol. Soc. Am.* **1969**, *15*, 237.
[24] P. Opdam, *Landscape Ecol.* **1991**, *5*, 93.
[25] J. V. Wells, M. E. Richmond, *Wildl. Soc. B* **1995**, *23*, 458.
[26] I. Hanski, *Nature* **1998**, *396*, 41.
[27] A. Terui, N. Ishiyama, H. Urabe, S. Ono, J. C. Finlay, F. Nakamura, *Proc. Natl. Acad. Sci. USA* **2018**, *115*, E5963.
[28] L. Laikre, F. Olsson, E. Jansson, O. Hössjer, N. Ryman, *Heredity* **2016**, *117*, 279.
[29] C. Thomas, *Conserv. Biol.* **1994**, *8*, 373.
[30] I. González-García, R. V. Solé, J. Costa, *Proc. Natl. Acad. Sci. USA* **2002**, *99*, 13085.
[31] D. Balcan, B. Gonçalves, H. Hu, J. J. Ramasco, V. Colizza, A. Vespignani, *J. Comput. Sci.* **2010**, *1*, 132.
[32] Q. Zhang, K. Sun, M. Chinazzi, A. P. y Piontti, N. E. Dean, D. P. Rojas, S. Merler, D. Mistry, P. Poletti, L. Rossi, M. Bray, M. E. Halloran, I. M. Longini, A. Vespignani, *Proc. Natl. Acad. Sci. USA* **2017**, *114*, E4334.
[33] D. J. Watts, R. Muhamad, D. C. Medina, P. S. Dodds, *Proc. Natl. Acad. Sci. USA* **2005**, *102*, 11157.
[34] S. C. Kramer, S. Pei, J. Shaman, *PLOS Comput. Biol.* **2020**, *16*, e1008233.
[35] L. Wang, X. Li, *Chin. Sci. Bull.* **2014**, *59*, 3511.
[36] H. Barbosa, M. Barthelemy, G. Ghoshal, C. R. James, M. Lenormand, T. Louail, R. Menezes, J. J. Ramasco, F. Simini, M. Tomasini, *Phys. Rep.* **2018**, *734*, 1.
[37] G. K. Zipf, *Am. Sociol. Rev.* **1946**, *11*, 677.
[38] X. Li, H. Tian, D. Lai, Z. Zhang, *Int. J. Environ. Res. Public Health* **2011**, *8*, 3134.
[39] P. McCullagh, J. A. Nelder, *Generalized Linear Models*, Routledge, Milton Park**2019**.
[40] S. A. Stouffer, *Am. Sociol. Rev.* **1940**, *5*, 845.
[41] F. Simini, M. C. González, A. Maritan, A.-L. Barabási, *Nature* **2012**, *484*, 96.
[42] M. Tang, Z. Liu, B. Li, *Europhys. Lett.* **2009**, *87*, 18005.
[43] S. Gómez, A. Fernández, S. Meloni, A. Arenas, *Sci. Rep.* **2019**, *9*, 2315.
[44] V. Colizza, R. Pastor-Satorras, A. Vespignani, *Nat. Phys.* **2007**, *3*, 276.
[45] V. Colizza, A. Vespignani, *J. Theoret. Biol.* **2008**, *251*, 450.
[46] J. D. Noh, H. Rieger, *Phys. Rev. Lett.* **2004**, *92*, 118701.
[47] R. Pastor-Satorras, A. Vespignani, *Phys. Rev. Lett.* **2001**, *86*, 3200.
[48] M. C. González, C. A. Hidalgo, A.-L. Barabási, *Nature* **2008**, *453*, 779.
[49] L. Alessandretti, P. Sapiezynski, V. Sekara, S. Lehmann, A. Baronchelli, *Nat. Human Behav.* **2018**, *2*, 485.
[50] L. Alessandretti, P. Sapiezynski, S. Lehmann, A. Baronchelli, *PLOS One* **2017**, *12*, e0171686.
[51] A. Wesolowski, N. Eagle, A. J. Tatem, D. L. Smith, A. M. Noor, R. W. Snow, C. O. Buckee, *Science* **2012**, *338*, 267.
[52] L. Lotero, R. G. Hurtado, L. M. Floría, J. Gómez-Gardeñes, *R. Soc. Open Sci.* **2016**, *3*, 150654.
[53] M. Macedo, L. Lotero, A. Cardillo, H. Barbosa, R. Menezes, in *Complex Networks XI* Springer, Cham **2020**, pp. 269–281.
[54] M. Macedo, L. Lotero, A. Cardillo, R. Menezes, H. Barbosa, *arXiv:2102.06619* **2021**.
[55] D. Balcan, A. Vespignani, *Nat. Phys.* **2011**, *7*, 581.
[56] D. Balcan, A. Vespignani, *J. Theor. Biol.* **2012**, *293*, 87.
[57] V. Belik, T. Geisel, D. Brockmann, *Eur. Phys. J. B* **2011**, *84*, 579.
[58] H. Coşkun, N. Yıldırım, S. Gündüz, *Sci. Total Environ.* **2021**, *751*, 141663.
[59] D. W. Wong, Y. Li, *PLOS One* **2020**, *15*, e0242398.
[60] N. Kadi, M. Khelfaoui, *Bull. Natl. Res. Centre* **2020**, *44*, 138.
[61] J. Gómez-Gardeñes, D. Soriano-Paños, A. Arenas, *Nat. Phys.* **2018**, *14*, 391.
[62] D. Soriano-Paños, L. Lotero, A. Arenas, J. Gómez-Gardeñes, *Phys. Rev. X* **2018**, *8*, 3.
[63] Eurostat, Passenger mobility statistics **2021**, https://ec.europa.eu/eurostat/statistics-explained/index.php?title=Passenger_mobility_statistics (accessed: December 2021).
[64] C. Granell, P. J. Mucha, *Phys. Rev. E* **2018**, *97*, 052302.
[65] P. Erdös, A. Rényi, In *The Structure and Dynamics of Networks*, Princeton University Press, Princeton **2011**, pp. 38–82.
[66] A.-L. Barabási, R. Albert, *Science* **1999**, *286*, 509.
[67] S. Gómez, A. Arenas, J. Borge-Holthoefer, S. Meloni, Y. Moreno, *Europhys. Lett.* **2010**, *89*, 38009.
[68] A. Wesolowski, C. O. Buckee, D. K. Pindolia, N. Eagle, D. L. Smith, A. J. Garcia, A. J. Tatem, *PLOS One* **2013**, *8*, e52971.
[69] United States Census. Bureau, https://data.census.gov/cedsci/ (accessed: September 2021).
[70] T. Louail, M. Lenormand, O. G. Cantu Ros, M. Picornell, R. Herranz, E. Frias-Martinez, J. J. Ramasco, M. Barthelemy, *Sci. Rep.* **2014**, *4*, 5276.
[71] S. Phithakkitnukoon, Z. Smoreda, P. Olivier, *PLOS One* **2012**, *7*, e39253.
[72] B. Hawelka, I. Sitko, E. Beinat, S. Sobolevsky, P. Kazakopoulos, C. Ratti, *Cartography Geogr. Inf. Sci.* **2014**, *41*, 260.
[73] S. Jiang, J. Ferreira, M. C. Gonzalez, *IEEE Trans. Big Data* **2017**, *3*, 208.
[74] A. Bassolas, H. Barbosa-Filho, B. Dickinson, X. Dotiwalla, P. Eastham, R. Gallotti, G. Ghoshal, B. Gipson, S. A. Hazarie, H. Kautz, O. Kucuktunc, A. Lieber, A. Sadilek, J. J. Ramasco, *Nat. Commun.* **2019**, *10*, 4817.
[75] S. Hazarie, D. Soriano-Paños, A. Arenas, J. Gómez-Gardeñes, G. Ghoshal, *Commun. Phys.* **2021**, *4*, 191.
[76] R. A. Marcus, *J. Phys. Chem. A* **2001**, *105*, 2612.
[77] A. S. Mata, S. C. Ferreira, *Phys. Rev. E* **2015**, *91*, 012816.
[78] S. C. Ferreira, R. S. Sander, R. Pastor-Satorras, *Phys. Rev. E* **2016**, *93*, 032314.
[79] J. Gómez-Gardeñes, S. Gómez, A. Arenas, Y. Moreno, *Phys. Rev. Lett.* **2011**, *106*, 128701.
[80] M. M. Norton, N. Tompkins, B. Blanc, M. C. Cambria, J. Held, S. Fraden, *Phys. Rev. Lett.* **2019**, *123*, 148301.
[81] D. Soriano-Paños, G. Ghoshal, A. Arenas, J. Gómez-Gardeñes, *J. Stat. Mech. Theory Exp.* **2020**, *2020*, 024006.
[82] C. Poletto, M. Tizzoni, V. Colizza, *Sci. Rep.* **2012**, *2*, 476.
[83] C. Poletto, M. Tizzoni, V. Colizza, *J. Theoret. Biol.* **2013**, *338*, 41.
[84] J. T. Matamalas, M. D. Domenico, A. Arenas, *J. R. Soc. Interface* **2016**, *13*, 20160203.
[85] A. Apolloni, C. Poletto, J. J. Ramasco, P. Jensen, V. Colizza, *Theor. Biol. Med. Model.* **2014**, *11*, 3.
[86] P. Bosetti, P. Poletti, M. Stella, B. Lepri, S. Merler, M. De Domenico, *Proc. Natl. Acad. Sci. USA* **2020**, *117*, 30118.
[87] Z. Ruan, M. Tang, C. Gu, J. Xu, *Chaos: Interdiscip. J. Nonlinear Sci.* **2017**, *27*, 103104.
[88] W. Cota, D. Soriano-Paños, A. Arenas, S. C. Costa, J. Gómez-Gardeñes, *New J. Phys.* **2021**, *23*, 073019.
[89] D. H. Silva, S. C. Ferreira, *J. Phys. Complex.* **2021**, *2*, 025011.
[90] J. Cardy, *Scaling and Renormalization in Statistical Physics*, Cambridge University Press, Cambridge**1996**.
[91] T. Vojta, *J. Phys. A. Math. Gen.* **2006**, *39*, R143.
[92] M. Henkel, H. Hinrichsen, S. Lübeck, *Non-Equilibrium Phase Transitions, Vol. 1*, Springer-Verlag, Berlin, Heidelberg**2009**.
[93] J. Marro, R. Dickman, *Nonequilibrium Phase Transitions in Lattice Models*, Cambridge University Press, Cambridge**2015**.
[94] M. a. Muñoz, R. Juhász, C. Castellano, G. Ódor, *Phys. Rev. Lett.* **2010**, *105*, 128701.
[95] P. Moretti, M. A. Muñoz, *Nat. Commun.* **2013**, *4*, 2521.

[96] W. Cota, G. Ódor, S. C. Ferreira, *Sci. Rep.* **2018**, *8*, 9144.
[97] L. Hébert-Dufresne, A. Allard, *Phys. Rev. Res.* **2019**, *1*, 013009.
[98] C. Castellano, R. Pastor-Satorras, *Phys. Rev. Lett.* **2010**, *105*, 21.
[99] A. V. Goltsev, S. N. Dorogovtsev, J. G. Oliveira, J. F. F. Mendes, *Phys. Rev. Lett.* **2012**, *109*, 12.
[100] P. Van Mieghem, *Comput. Commun.* **2012**, *35*, 1494.
[101] Y. Wang, D. Chakrabarti, C. Wang, C. Faloutsos, in *Proceedings of the 22nd Int. Symp. Reliab. Distrib. Syst. 2003*, IEEE, Piscataway, NJ **2003**, pp. 25–34.
[102] F. Chung, L. Lu, V. Vu, *Proc. Natl. Acad. Sci. USA* **2003**, *100*, 6313.
[103] R. Pastor-Satorras, C. Castellano, *Sci. Rep.* **2016**, *6*, 18847.
[104] H. K. Lee, P.-S. Shim, J. D. Noh, *Phys. Rev. E* **2013**, *87*, 062812.
[105] S. Chatterjee, R. Durrett, *Ann. Probab.* **2009**, *37*, 2332.
[106] R. Pastor-Satorras, A. Vespignani, *Phys. Rev. E* **2001**, *63*, 066117.
[107] S. C. Ferreira, C. Castellano, R. Pastor-Satorras, *Phys. Rev. E* **2012**, *86*, 041125.
[108] M. Boguñá, R. Pastor-Satorras, *Phys. Rev. E* **2002**, *66*, 047104.
[109] D. H. Silva, S. C. Ferreira, W. Cota, R. Pastor-Satorras, C. Castellano, *Phys. Rev. Res.* **2019**, *1*, 033024.
[110] M. Boguñá, C. Castellano, R. Pastor-Satorras, *Phys. Rev. Lett.* **2013**, *111*, 068701.
[111] W. Cota, A. S. Mata, S. C. Ferreira, *Phys. Rev. E* **2018**, *98*, 012310.
[112] R. M. Anderson, R. M. May, *Infectious Diseases of Humans: Dynamics and Control, Dynamics and Control*, Oxford University Press, New York, NY **1992**.
[113] M. Catanzaro, M. Boguñá, R. Pastor-Satorras, *Phys. Rev. E* **2005**, *71*, 027103.
[114] D. H. Silva, S. C. Ferreira, *Chaos An Interdiscip. J. Nonlinear Sci.* **2018**, *28*, 123112.
[115] G. S. Costa, S. C. Ferreira, *Phys. Rev. E* **2020**, *101*, 022311.
[116] J. Gómez-Gardenes, V. Latora, *Phys. Rev. E* **2008**, *78*, 065102.
[117] A. Fronczak, P. Fronczak, *Phys. Rev. E* **2009**, *80*, 016107.
[118] R. Sinatra, J. Gómez-Gardenes, R. Lambiotte, V. Nicosia, V. Latora, *Phys. Rev. E* **2011**, *83*, 030103.
[119] R. Pastor-Satorras, A. Vespignani, *Phys. Rev. E* **2002**, *65*, 036104.
[120] R. Cohen, S. Havlin, D. Ben-Avraham, *Phys. Rev. Lett.* **2003**, *91*, 247901.
[121] Z. Wang, C. T. Bauch, S. Bhattacharyya, A. D'Onofrio, P. Manfredi, M. Perc, N. Perra, M. Salathé, D. Zhao, *Phys. Rep.* **2016**, *664*, 1.
[122] M. Newman, *Networks*, Oxford University Press, New York, NY **2010**.
[123] W. Pan, G. Ghoshal, C. Krumme, M. Cebrian, A. Pentland, *Nat. Commun.* **2013**, *4*, 1961.
[124] M. Batty, *The New Science of Cities*, MIT Press, Cambridge, MA **2017**.
[125] M. Barthelemy, *The Structure and Dynamics of Cities: Urban Data Analysis and Theoretical Modeling*, Cambridge University Press, Cambridge **2017**.
[126] M. Barthelemy, *Nat. Rev. Phys.* **2019**, *1*, 406.
[127] M. Kardar, *Statistical Physics of Fields*, Cambridge University Press, Cambridge **2014**.
[128] E. Valdano, M. R. Fiorentin, C. Poletto, V. Colizza, *Phys. Rev. Lett.* **2018**, *120*, 6.
[129] T. Day, S. Gandon, *Ecol. Lett.* **2007**, *10*, 876.
[130] N. H. Barton, *Genet. Res.* **1993**, *62*, 149.
[131] M. C. Whitlock, *Genetics* **2003**, *164*, 767.
[132] D. Mistry, M. Litvinova, A. P. y Piontti, M. Chinazzi, L. Fumanelli, M. F. Gomes, S. A. Haque, Q.-H. Liu, K. Mu, X. Xiong, M. E. Halloran, I. M. Longini Jr, S. Merler, M. Ajelli, A. Vespignani, *Nat. Commun.* **2021**, *12*, 323.
[133] K. Prem, A. R. Cook, M. Jit, *PLOS Comput. Biol.* **2017**, *13*, e1005697.
[134] J. T. Chen, N. Krieger, *J. Public Health Manag. Pract.* **2021**, *27*, S43.

David Soriano-Paños is a postdoctoral fellow at Instituto Gulbenkian de Ciência. His works mainly focuses on the study of complex networks, epidemic modeling, and the characterization of human mobility.

Wesley Cota is a postdoctoral fellow at the Physics Department of the Universidade Federal de Viçosa, his work focuses on fundamental aspects of epidemic spreading models on complex networks, real-world applications with high-resolution data-driven models coupling human mobility and contact patterns, and echo chamber effects on Twitter networks.

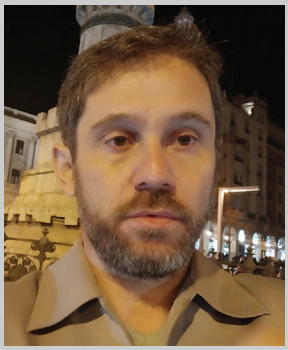

Silvio C. Ferreira is full Professor at the Physics Department of the Universidade Federal de Viçosa, CNPq research fellow, and member of the National Institute of Science and Technology for Complex Systems. His research is devoted to several aspects of dynamical complex systems, mainly focused on epidemic spreading, opinion formation, and critical phenomena on the top of complex networks.

Gourab Ghoshal is an Associate Professor of Physics at the University of Rochester, with joint appointments in the Departments of Computer Science and Mathematics. His research is in the field of Complex Systems writ large, including the theory and applications of complex networks, non-equilibrium statistical physics, game theory, econophysics, dynamical systems, and the origins of life.

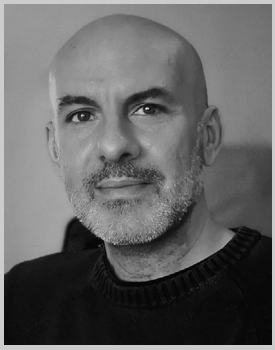

Alex Arenas is full Professor at Universitat Rovira i Virgili. In 2019, he was elected as Fellow of the American Physical Society, in 2020, he has was elected Fellow of the Network Science Society, and in 2021 he got the award—Mathematics and Society—from the Fundacio Ferran Sunyer i Balaguer. His works focus on applying statistical physics and nonlinear dynamics to real-world complex systems, with special interest in the physics of epidemics, synchronization and urban systems.

Jesús Gómez-Gardeñes is an Associate Professor at the University of Zaragoza where he leads the group of theoretical and applied modeling of the Institute for Bicomputation and Physics of Complex Systems. His works focus on applying statistical physics and nonlinear dynamics approaches to shed light on the basic mechanisms and interactions that shape the collective behavior of real-world complex systems.